POLEWARD PROPAGATING WEATHER SYSTEMS IN ANTARCTICA

by

Jessica A. Staude

A THESIS SUBMITTED IN PARTIAL FULFILLMENT OF THE REQUIREMENTS FOR THE DEGREE OF

Master of Science
(Atmospheric and Oceanic Sciences)

at the

UNIVERSITY OF WISCONSIN-MADISON

2007

Abstract

Antarctica has some of the most hazardous weather on Earth. The continent is known for its extreme weather including bitterly cold temperatures and brutal winds. The introduction of satellite coverage over the continent and Southern Ocean for weather research and operational forecasting has provided new insight into the patterns and origins of these harsh conditions. However, forecasting for travel across the continent is still difficult, especially in West Antarctica. In this study satellite imagery is used to determine impact times of weather systems over West Antarctica. Prior gaps in satellite coverage have impeded forecasting abilities, and real time data from automated weather stations (AWS) is limited because of the small number of stations in this region. The creation of Antarctic satellite composite images in 1992 has allowed for a comprehensive compilation of weather data around the continent and surrounding areas from a hemispheric view.

In this study, ten years of Antarctic composite satellite images from 1992-2002 are examined for poleward propagating weather systems in West Antarctica. These large scale synoptic events transport clouds onto the continent and affect local weather. These cloud mass systems are counted on a monthly basis, examined for long-term periodicity, and the temporal distribution of the systems is compared against climate indices. Over the 10-year period, Marie Byrd Land had a peak number (11 occurrences) in June, while Ellsworth Land had a peak of 11 occurrences in September. Ellsworth Land also had more CMT events (190) than Marie Byrd Land (165). The majority of the CMT events in both sectors occurred for a period of two to three days, with over 75 percent of CMT events having a length of five or less days.

A moderately significant relationship between the poleward propagating systems in West Antarctica and the El Niño-Southern Oscillation (ENSO) is found; however, most comparisons reveal no significant correlation. Case studies using AWS surface data verify the onset of conditions associated with systems identified in the composite images. The results suggest ways to improve seasonal forecasting over West Antarctica.

Table of Contents

List of Tables

List of Figures

1. Introduction

Antarctica is an isolated continent with unique meteorological conditions. Brutal storms and harsh winds are common for those who travel to the continent for research and exploration. For many years, researchers have been attempting to understand the weather and climate of this harsh continent. Since the climate is so brutal, the collection of weather observations has occurred at only sparsely scattered locations, mostly on the coast of the continent from manned stations.

Studies have been done using data from manned stations across the continent including one on the Antarctic climate record and ENSO (Smith and Stearns, 1993). Unmanned Antarctic Automated Weather Stations (AWSs) were first installed in 1980, allowing valuable meteorological information to be retrieved in many remote locations (Stearns et al., 1993). Data from AWS units has are accurate and consistent enough for research studies, such as examining the relationship between climate anomalies and the Southern Oscillation (Smith and Stearns, 1993). However, even in 2001, there were still large gaps in the coverage, especially in West Antarctica (Figure 1).

Forecasting has always been a problem for surviving and traveling on the continent. In recent years, flights have been postponed by cyclonic activity affecting locations for days or even weeks. In one case, a group of scientists remained at the West Antarctic Ice Sheet (WAIS) Divide site for several weeks because of unsafe weather for travel at their location. Delays such as these not only hinder research activities at the main bases, but can affect the usage of planes for specific-site research.

Satellites have added a whole new set of observations that fill in the gaps between surface stations and have proven extremely useful in understanding the drivers of Antarctic climate and its effects on local weather. Early uses of satellite imagery involved case studies with the goal to improve weather forecasting across the continent through the use of archived data (Kermann and Frame, 1966; Keith and O'Neal, 1967; Godin, 1977). Research and forecasting across Antarctica has been greatly benefited by the introduction of science quality satellite imagery and the increase in number of satellites with coverage over the continent. Researchers have been able to use new satellite data products, such as temperature and water vapor profiles to examine smaller-scale features across the continent including katabatic winds, one of the most difficult features to forecast (Lazzara et al., 2003a). Polar orbiting satellites have been useful in identifying and monitoring mesoscale cyclone genesis and movement across the continent, especially with improved sensors and image resolution (Key et al., 2001; Wang and Key, 2002; Carrasco et al., 2003; Lazzara et al., 2003a).

The addition of Antarctic composite satellite images in 1992 has been a huge asset to research and forecasting operations (Stearns and Lazzara, 1999). These images offer a view of clouds and their motion about the Southern Hemisphere, and specifically their advection or transport onto the Antarctic continent. The composites consist of data collected from a combination of over twenty different geostationary and polar orbiting satellites throughout the 10 year time period. When viewing the Antarctic composites, it is clear that extended periods exist when clouds from storm systems or other cloud masses are transported nearly perpendicularly onto specific regions of the Antarctic (Stearns and Lazzara, pers. comm., 2001). The goal of this study is to analyze when and where these poleward propagating systems occur, explore patterns and determine when these systems have the greatest impact. This paper covers the methods used to view, obtain, and analyze the satellite data for those 10 years, as well as a brief discussion on the initial results of the analysis. Chapter 2 contains a general overview of Antarctica and background information, as well as previous research on climate signal events. Chapter 3 discusses the different types of data used in support of this study. Chapter 4 describes poleward propagating systems and "cloud mass transport events" as well as the collection method. Chapter 5 discusses the results of this study, and Chapter 6 summarizes the conclusions of the analysis and provides information on future work.

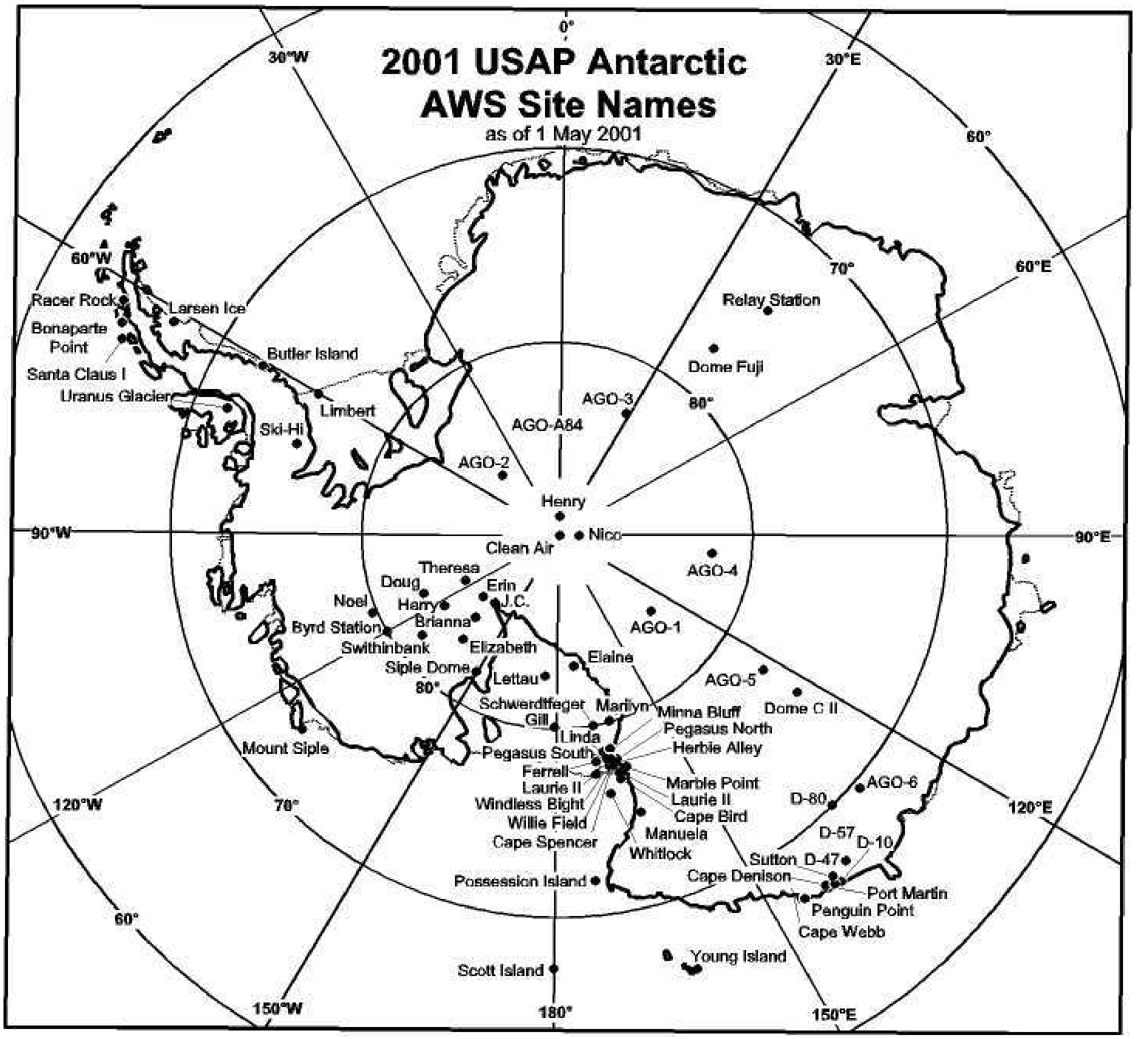

Figure 1. A map of Antarctica showing all operating AWS units in 2001 (from Keller et al., 2007).

2. Background

Antarctica is the coldest, driest, and windiest continent on the planet. These harsh meteorological conditions make it difficult to take consistent, accurate meteorological measurements. The weather and climate across the continent is unique in many different aspects. This section provides general information on the Antarctic continent and background work dealing with related climate and cloud mass research.

2.1 About Antarctica

Antarctica is the Earth's southernmost continent, comprising about 10 percent of the land surface and 90 percent of the world's fresh water ice. It has an area of approximately 1.4×10^7 km^2, making it the fifth largest continent on Earth (King and Turner, 1997). Antarctica has three main geographic regions: East Antarctica, West Antarctica, and the Antarctic Peninsula (Figure 2).

East Antarctica is the largest of the regions and is dominated by the Antarctic plateau, one of the largest deserts in the world with an average elevation above 2 km (Schwerdtfeger, 1984; King and Turner, 1997). The plateau exists in the form of an ice sheet which covers most of the continent, and is thickest in East Antarctica. East and West Antarctica are separated by the Transantarctic Mountain range. West Antarctica is the second largest region in Antarctica and is generally lower in elevation than East Antarctica (King and Turner, 1997). West Antarctica has the Ross Ice Shelf, an extremely large floating piece of ice. Ice shelves can calve large icebergs into the surrounding seas, a common feature of the Southern Ocean. One of the largest icebergs to date broke off in 2000 from the Ross Ice Shelf, with an area of approximately 10,000 km^2 (Arrigo, 2002).

The smallest region is the Antarctica Peninsula, a mountainous barrier extending northward from the main mass of the continent, and is the only region that extends outside the Antarctic Circle (King and Turner, 1997).

2.2 Antarctic Weather Patterns

Three main climatological weather features of particular interest around Antarctica are conveyed through mean sea level (MSL) pressure charts[1] (King and Turner, 1997). The three features are a circumpolar trough of low pressure surrounding Antarctica at a mean latitude of 66°S, a weak surface anticyclone over the Antarctic continent, and departures within the circumpolar trough via three low pressure centers around the continent. The circumpolar trough is at its strongest as well as closest to the continent in the spring and autumn, resulting from the high level of cyclonic activity around the coast of the continent (King and Turner, 1997).

Geopotential height fields illustrate another important feature of the Antarctic continent, a cyclonic vortex centered over the Ross Ice Shelf (Figure 3). At 500 hPa, above the surface of the continent at all areas, the flow takes the form of a vortex, with the mean patterns indicating the path around the center of the vortex flows onto the continent in West Antarctica, slightly west of the Ross Ice Shelf and flow off of the continent east of the Ross Ice Shelf, close to East Antarctica during the summer. In winter, the flow onto Antarctica shifts westward, onto the eastern edge of Marie Byrd Land. Higher geopotential height levels illustrate the displacement and strengthening of the vortex towards the South Pole

---

[1] Note that the surface pressure is around 600 hPa or less, making MSL pressures over the continent essentially fictitious.

(King and Turner, 1997). This flow is related to the poleward propagating systems found in West Antarctica which are discussed in detail in later chapters.

Cyclones over the Antarctic continent and the Southern Ocean contribute to the general circulation of the atmosphere. In the Southern Hemisphere, standing waves are much more barotropic than in the Northern Hemisphere, so cyclones are responsible for a majority of the poleward transport of heat and momentum. The frequent cyclonic activity in the southern latitudes is responsible for the formation of the circumpolar trough (Van Loon, 1979; King and Turner, 1997).

West Antarctica is of great interest to cyclone development. Over West Antarctica, where the topography is lower, there is a high density of cyclone activity, particularly in the Amundsen and Bellingshausen Seas (Jones and Simmonds, 1993). Additionally, a peak in cyclone centers was found over the eastern area of the Ross Ice Shelf (Taljaard, 1967).

2.3 Related work

Several studies in the past have focused on Antarctic climate with ENSO as well as cyclonic activity and distribution across the continent. An important study done by Smith and Stearns (1993) examined relationships between Antarctic temperature and pressure anomalies and the Southern Oscillation (SO). One segment of their results showed that composite annual pressure anomaly (CAPA) and composite annual temperature anomaly (CATA) present before a minimum in the Southern Oscillation Index (SOI) resulted in the strengthening of a trough over the Ross Ice Shelf. Additionally, they found a significant relationship between temperature and pressure anomalies and the SOI (Smith and Stearns, 1993).

Mesoscale cyclone activity has been of great interest over the continent. Carrasco et al. (2003) not only found a significant region of mesoscale cyclonic activity over West Antarctica, but state that their source areas are not clearly identified. They suggest regions of cyclogenesis exist north of the Bellingshausen Sea and in the region of the Amundsen Sea. Additionally, they discovered the area over the Bellingshausen Sea favors the formation and development of mesoscale cyclonic perturbations due to an unstable environment, possibly associated with the circumpolar vortex centered northeast of the Ross Ice Shelf (Carrasco et al., 2003).

A link between ENSO and weather systems has also been described by Sinclair et al. (1997). They examined the month-to-month variations in Southern Hemisphere (SH) weather system tracks and found a 20 percent increase in cyclones during El Niño winters over the subtropical Pacific towards South America. They also found frequent blocking anticyclones south and southeast of New Zealand during La Niña summers (Sinclair et al., 1997).

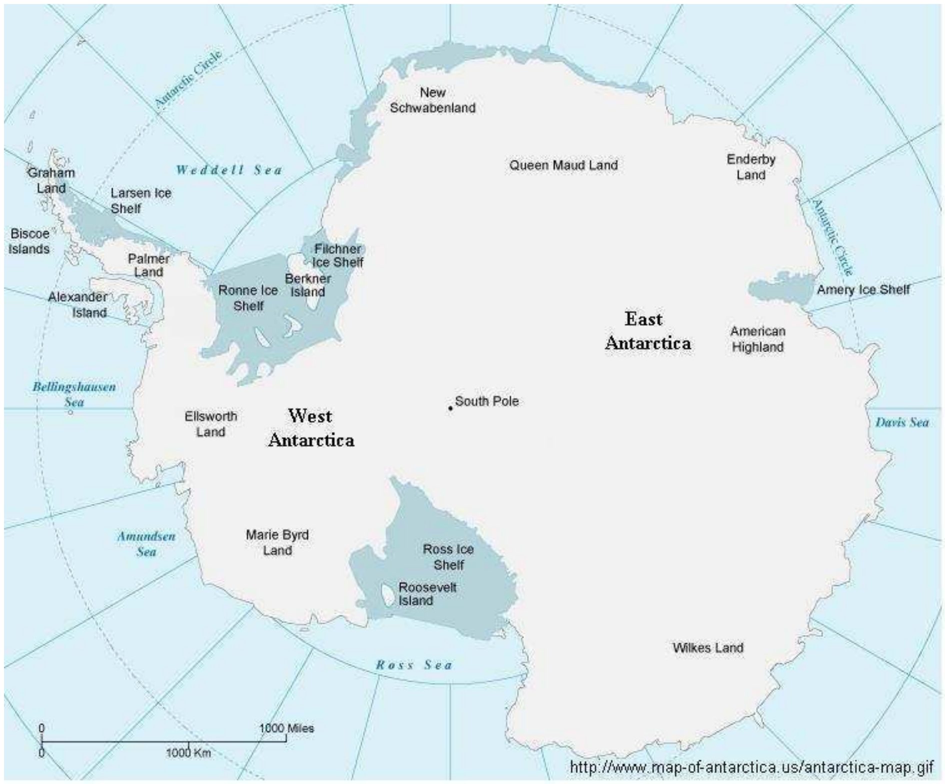

Figure 2. Map of Antarctica showing geographical locations (from http://www.map-of-antarctica.us/antarctica-map.gif).

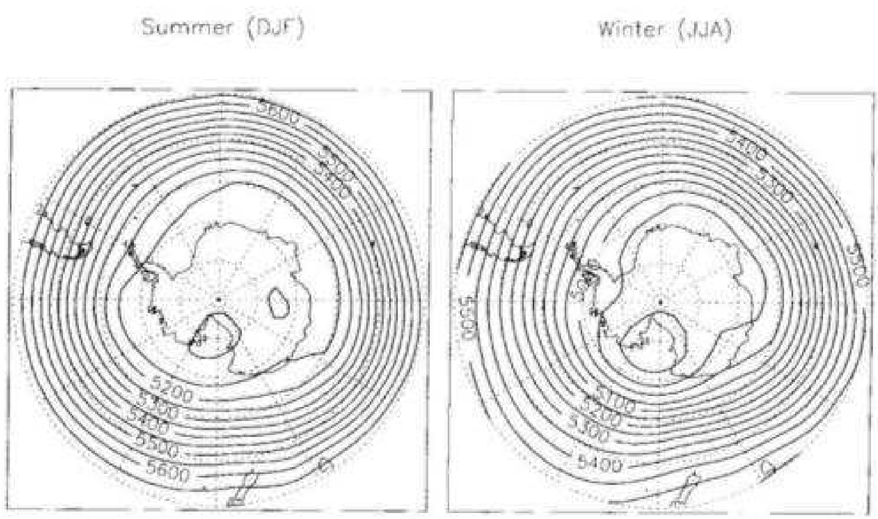

Figure 3. Average 500 hPa geopotential heights during the summer and winter months from the Australian Bureau of Meteorology for the period 1972-91 (from King and Turner, 1997).

3. Data

This study uses data from many sources. In this section, the collection and creation of this data is described, and background behind the satellite images, climate indices, real-time data from automatic weather stations, and reanalysis data utilized in this study is discussed.

3.1 Composite Satellite Images

The Antarctic composite satellite images used during this study were begun in October of 1992 and are developed at the Antarctic Meteorological Research Center (AMRC) at the University of Wisconsin-Madison (Stearns and Lazzara, 1999). Over twenty different geostationary and polar-orbiting satellites from around the world have been used in the making of the composite images throughout the 10-year period between October 1992 and October 2002.

Geostationary satellites remain at a fixed altitude of approximately 36,000 km above the equator, with an orbit period that matches that of the Earth. Since the orbit of Earth and the satellite are the same, the satellite constantly observes the same region of the globe. Geostationary satellite imagery was used from three different organizations:

1. The National Environmental Satellite, Data, and Information Service (NESDIS), part of the National Oceanic and Atmospheric Administration (NOAA) in the United States, has two main Geostationary Operational Environmental Satellite (GOES) satellite coverage areas. GOES-East monitors North and South America and the western Atlantic Ocean, and GOES-West monitors North and South American and the eastern

Pacific Ocean. Throughout the 10-year period GOES-7 through GOES-10 encompassed these two satellite coverage regions (Menzel and Purdom, 1994).

2. The Japan Meteorological Agency (JMA) has the Geostationary Meteorological Satellite (GMS) that covers eastern Asia, Australia, the western Pacific Ocean, and the eastern Indian Ocean. GMS-4 and GMS-5 were included in the satellite composites during this time period.
3. The European Organization for the Exploitation of Meteorological Satellites (EUMETSAT), has two main satellite coverage regions that monitor Europe, Africa, Asia, the Indian Ocean, and the Atlantic Ocean. Meteosat-5 and Meteosat-7 were used over these regions in the 10-year time frame.

Polar orbiting satellites have an orbit that passes above, or nearly above both of Earth's poles at an altitude between 800 and 900 km and an orbital period between 98 and 102 minutes. Their data swath is approximately 3,000 km wide, and with each orbit, a new longitudinal region is observed over the equator. Polar orbiting satellites from two different organizations were utilized in the composite image; the Defense Meteorological Satellite Program (DMSP), a Department of Defense (DoD) program run by the Air Force Space and Missile Systems Center (SMC), and NESDIS. DMSP satellites lie at an altitude of 830 km, and have a 101-minute period in a sun-synchronous near-polar orbit. Sun-synchronous orbits combine altitude and inclination to create an orbit that passes over any given point on Earth at the same local time. DMSP-11 through DMSP-15 images are used in the satellite composites. At an altitude between 830 and 870 km, Polar Orbiting Environmental Satellites (POES) satellites from NESDIS are also in sun-synchronous orbits, with an orbital period of approximately 102 minutes. Images from NOAA-11 through NOAA-17 are used in the 10 year period of the satellite composites.

The satellite bands used in the composite images were from the infrared spectrum near the 11 µm atmospheric window. The 11 µm band is considered an atmospheric window because there is little atmospheric absorption, allowing surface features to be seen clearly in cloud free conditions, as well as the detection of high clouds in the atmosphere. Additionally, reflected solar radiation is negligible, creating no bias between daytime and nighttime hours. Since the spectral response function of the bands varies slightly from satellite to satellite, actual values of the infrared bands constituting the composite images are in a .8 µm range between 10.7 and 11.5 µm. Table 1 lists the wavelengths of each band used in the satellite composite images.

Several different instruments were used over the years on the various satellites. GOES-7 is the only GOES satellite used in the composites that contains the Visible Infrared Spin-Scan Radiometer (VISSR) Atmospheric Sounder (VAS). The VAS is a dual-band spin-scanning imaging device, along with a six band infrared sounder. GOES-8 through GOES-10 satellites have an imaging radiometer with one visible and four infrared bands (Menzel and Purdom, 1994). The GMS satellites carry the VISSR instrument with two channels in the visible and infrared ranges. METEOSAT satellites have an imaging radiometer with one visible and two infrared bands. The DMSP satellites carry the Operational Linescan System (OLS) instrument, which obtains visible and infrared imagery. The OLS contains an infrared telescope sensitive to radiation in the infrared range between 10.0 and 13.4 µm. NOAA satellites contain the Advanced Very High Resolution Radiometer (AVHRR) instrument which encompasses three different types of data; High

Resolution Direct Readout AVHRR (HRPT), Recorded HRPT AVHRR (LAC), and Reduced Resolution Recorded HRPT AVHRR (GAC).

The creation of the satellite composite images is accomplished with the Man computer Interactive Data Access System (McIDAS), which has been in development since 1973 by the Space Science and Engineering Center (SSEC) at the University of Wisconsin-Madison (Figure 4). The McIDAS-X package is a compilation of software used for visualization and analysis of many different types of geophysical data, including satellite imagery. The vast varieties of functions McIDAS-X can perform include acquiring, displaying, analyzing and interpreting data (Lazzara et al., 1999).

The process of the creation of the composite images begins with the acquisition of satellite images. Selected infrared images are gathered in a +/- 50 minute time range around every three synoptic hours, creating eight images per day. The images are remapped in McIDAS to merge several images together to create a composite mosaic. Parts of outer space captured by the satellites are removed from the images, and any bad satellite lines are cleaned up. The final step merges the satellite images together to form a composite image of the entire continent of Antarctica and the surrounding region of the Southern Hemisphere. The procedure combines the geostationary images first, and then merges the polar orbiting images on top. When the merging procedure encounters overlapping images, a conditional minimum is used, resulting in the lower brightness values on the top of the image. Because the geostationary images are first, followed by the polar orbiting, the polar orbiting satellite images generally take precedence on top in the composites (Lazzara et al., 2003b).

At the AMRC, an Antarctic Composite video containing the entire dataset of the composite images was made to keep a record of the data, as well as to create a composite movie that could be viewed for research. The tape was made by adding larger, more visible labels to each composite image listing the day and time, and then recording the composite images in groups and editing them together. The tape was eventually converted to DVD to increase the longevity of the media.

3.2 Climate Signals and Indices

Climate indices are used in research to attempt to characterize various climate mechanisms that affect daily weather across the globe. Several different long-term climate signals were examined in this study. This section will provide background information on each climate signal, as well as the indices used in this study.

3.2.1 El Niño-Southern Oscillation

The Southern Oscillation is often referenced with El Niño, combining the two terms together as the El Niño-Southern Oscillation (ENSO). Various attempts have been made to create a working definition of El Niño; however, there is not one clear-cut definition, since the past attempts to define El Niño have not led to a general acceptance in the community (Trenberth, 1997). For example, one definition refers to El Niño as the annual weak warm ocean current running southward along the coast of Peru and Ecuador around Christmastime, lasting a few weeks to a month or more. More recently, the term El Niño has become associated with the unusually large warming occurring every three to seven years (Trenberth, 1997).

The Walker circulation, an atmospheric circulation at the equatorial Pacific Ocean, is indicative of an El Niño event when it weakens. In normal conditions, the Walker circulation encompasses trade winds blowing warm, moist air west across the tropical Pacific, creating a sea surface temperature (SST) gradient between 3 and 6 K, with warmer waters to the west and cool waters to the east. When the air reaches the warm western Pacific Ocean, it rises and becomes associated with a region of low pressure and precipitation. The air reaches high levels of the atmosphere and travels eastward before descending over the eastern Pacific Ocean bringing high pressure and dry conditions. During an El Niño event, the Walker circulation weakens or reverses, and SSTs in the eastern Pacific Ocean are warmer than normal. In the west, SSTs near the dateline are at or slightly below normal, diminishing the east-west temperature gradient. Furthermore, the regions of heavy rainfall shift eastward, resulting in drought conditions in Indonesia and adjacent regions, while the equatorial central Pacific experiences heavy rainfall. The trade winds weaken or shift to the west near and to the west of the date line (Rasmusson and Wallace, 1983).

The Southern Oscillation (SO) is the atmospheric component of ENSO. The term was introduced in 1924 by Sir Gilbert Walker to describe the complex climatological relations in the Indian and Pacific Oceans. It is defined as the see-saw pattern of reversing surface air pressure between the Indian and Pacific Oceans in the tropics and subtropics. The main evidence for the SO is the work done by Walker (1923, 1924) and Walker and Bliss (1928). In 1932, Walker and Bliss define the SO “In general terms, when pressure is high in the Pacific Ocean, it tends to be low in the Indian Ocean from Africa to Australia; these conditions are associated with low temperatures in both these areas, and rainfall varies in the opposite direction to pressure. Conditions are related differently in winter and summer…" (Walker and Bliss, 1932). The period of the SO is irregular and varies between 2 and 10 years (Troup, 1965; Trenberth, 1984).

The Southern Oscillation is monitored by an index formed from surface pressure differences across the South Pacific (Troup, 1965; Chen, 1982; McBride and Nicholls, 1983; Trenberth, 1984; Ropelewski and Jones, 1987). The Southern Oscillation Index (SOI) was devised by Walker, in which the sign and magnitude of the index indicate the anomalies of the associated elements in the region between the Indian and Pacific Oceans. Walker's description of the SOI indicates that it is high when pressure is high over the Pacific and low over the Indian Ocean regions. The Troup SOI is used in this study, which is the normalized mean sea level pressure anomaly difference between Tahiti, French Polynesia (17.5° S, 149.6° W) and Darwin, Australia (12.4° S, 130.9° E) (Troup, 1965). The SOI is obtained from the Australian Bureau of Meteorology (see http://www.bom.gov.au/climate/current/soihtm1.shtml). The SOI is a simple measure of the strength and phase of the Southern Oscillation and also indicates the phase of the Walker circulation. A large positive SOI index indicates a La Niña year, while a large negative value is representative of an El Niño year (Figure 5).

The Niño-3.4 Index is another ENSO indicator, based on sea surface temperatures. It was developed after the four original "Niño" regions selected by the Climate Analysis Center (CAC, now known as the Climate Prediction Center (CPC)) in the early 1980s to observe the SST part of ENSO (Figure 6; Barnston and Chelliah, 1997). It is defined as the average SST anomaly in the region between 5° N and 5° S from 170° W to 120° W, based upon the fact that the correlation between the SOI-defined ENSO events are stronger with the Niño-3.4 index than the Niño-3 index (Figure 7; Barnston and Chelliah, 1997; Hanley et al., 2003). The Niño-3.4 index is obtained from the Royal Netherlands Meteorological Institute (see http://climexp.knmi.nl/data/inino5.dat).

3.2.2 Antarctic Oscillation

The Antarctic Oscillation (Gong and Wang, 1999; AAO), also known as the high latitude mode (Rogers and van Loon, 1982), or the Southern Annual Mode (Limpasuvan and Hartmann, 1999; SAM), is a mode of atmospheric variability in the Southern Hemisphere. Walker first discovered the AAO in 1928, stating "Just as in the North Atlantic there is a pressure opposition between the Azores and Iceland,…,there is an opposition between the high pressure belt across Chile and the Argentine on the one hand, and the low pressure area of Weddell Sea and the Bellingshausen Sea on the other." (Walker, 1928). The AAO measures north-south shifts in atmospheric mass between the polar regions and the middle latitudes. It is characterized by pressure anomalies of one sign centered in the Antarctic and anomalies of the opposite sign centered about 40-50S.

The AAO is the leading empirical orthogonal function (EOF) in many atmospheric fields, including geopotential height, surface pressure, surface temperature, and zonal wind (Thompson and Wallace, 2000). The AAO index is defined as the difference between the normalized monthly zonal MSLP at 40° S and 60° S (Figure 8). These two latitudes were chosen by Gong and Wang based upon the calculated magnitude (-0.59) and statistical significance (<1%) of the correlation coefficient between them. It is created by projecting the daily (00Z) 700mb height anomalies poleward of 20°S onto the loading pattern of the AAO. This loading pattern is defined as the leading mode of EOF analysis of monthly mean 700 hPa height during a period from 1979-2000. Since the loading pattern is obtained using monthly means, the AAO index is calculated by normalizing by the standard deviation of the monthly index. The AAO is in its positive (negative) phase when pressures over Antarctica are relatively low (high) compared to the mid-latitudes (Gong and Wang, 1999).

3.3 Antarctic Automated Weather Stations

Data from several Antarctic Automated Weather Stations (AWSs) were used in case studies focusing on several poleward propagating systems in West Antarctica. Many of these stations were placed in remote areas of the continent, facing harsh conditions over the years. The AWS project at the University of Wisconsin-Madison installed a total of four U.S. AWS units across Antarctica during its first year in 1980 (Stearns et al., 1993). As of 2002, there were approximately 60 active stations operating across Antarctica.

The AWS units collect several different meteorological measurements, including air temperature, pressure, wind speed and wind direction. More recently, relative humidity and vertical temperature difference have been added to newer AWS units. The temperature, wind speed, wind direction and relative humidity are measured at a nominal height of three meters, while the pressure is measured in an enclosed box at a nominal height of 1.75 meters. The addition of snow by accumulation or drifting can affect the height of the tower at the station site, which is generally three meters (Stearns et al., 1993).

Onboard the AWS units are small computers which control the operating cycle, and may store the meteorological data collected from the unit. The data are transmitted via the ARGOS data collection system (DCS). The ARGOS DCS are onboard National Oceanic and Atmospheric Administration (NOAA) polar orbiter satellites, and transmit data received from the AWS units to various ground stations via direct broadcast. This method is the only way to transmit the data, and can only occur when the satellites are above the horizon at the AWS site, which happens for 10-15 minutes for approximately 12 of the 14 NOAA orbits during a 24 hour period, depending on the location of the AWS unit. The orbits work out to approximately one satellite in view of an AWS site every 50 minutes. However, since there are times when the satellites are out of range, data can be occasionally lost if the transmission occurs when there are no NOAA satellites in range (Stearns et al., 1993).

Many of the AWS units are powered by six to twelve 40 ampere-hour 12 volt gel-cell batteries charged by one or two 10 Watt solar panels. The units near the South Pole require 12 batteries and two solar panels to keep the station operational. This system generally keeps the station operational year-round, but an occasional lack of power can occur from drained or older batteries, as their capacity decreases with time. Other data problems can occur from malfunctioning equipment, especially the wind system, the most vulnerable part of the AWS. For example, high wind speeds and frost build up can cause missing or incorrect data (Stearns et al., 1993).

3.4 Reanalysis Data

The National Centers for Environmental Prediction (NCEP, formerly the National Meteorological Center (NMC)) and the National Center for Atmospheric Research (NCAR) began cooperating in a global reanalysis project in 1991. The goal of the project was to produce a 40-year record of global analyses of atmospheric fields that was of research quality, and was to be used by the research and climate monitoring communities (Kalnay et al., 1996). The motivation for this reanalysis project started from apparent “climate changes” resulting from changes introduced into the NMC operational Global Data Assimilation System (GDAS, Kalnay et al., 1996). In order to produce the record, recovery and quality control was performed for land surface, ship, rawinsonde, pibal, aircraft, and satellite data, as well as other data types. The project used a state-of-the-art analysis and forecast system, and performed data assimilation with the past data.

Scientists at NCEP designed the reanalysis system, while those at NCAR performed the majority of the data collection, obtaining several special datasets that were not widely available. The reanalysis system consists of a data decoder and quality control (QC) preprocessor, a data assimilation module with an automatic monitoring system, and an archive module. Currently, the original 40-year record of reanalysis data from the period 1957 – 1996 has been completed, as well as extended to the years 1948 to the present using the NMC Climate Data Assimilation System (CDAS). The data was reformatted into the World Meteorological Organization’s (WMO) binary universal format representation (BURF) format and placed into several archives (Kalnay et al., 1996).

Satellite	Wavelength used in Composites (µm)
GOES-7	11.2
GOES-8 – GOES-10	10.7
GMS-4 – GMS-5	11.0
Meteosat-5, Meteosat-7	11.5
DMSP-11 – DMSP-15	11.0
NOAA-11 – NOAA-17	10.8

Table 1. A listing of the wavelengths used in the satellite composite images for each satellite.

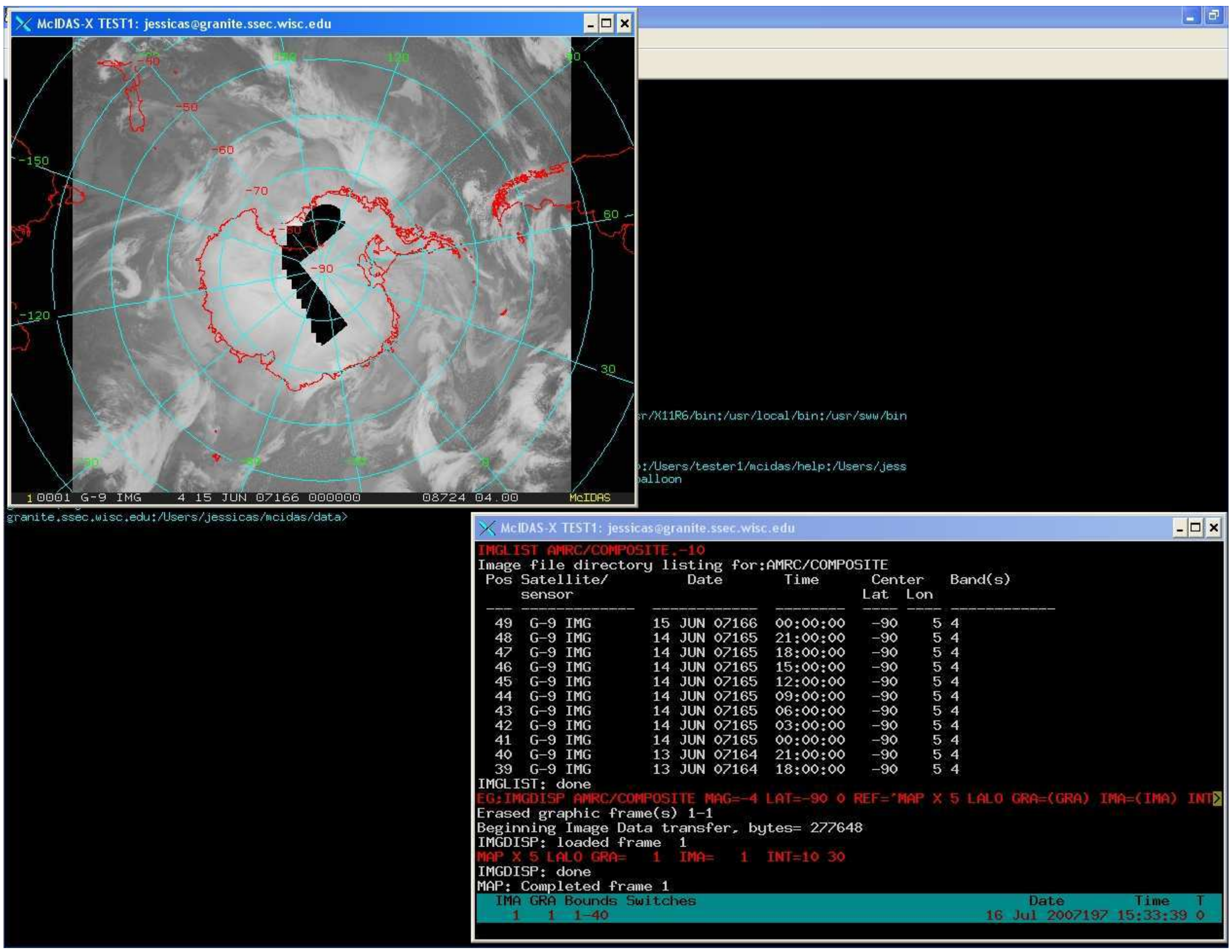

Figure 4. The McIDAS-X software in use.

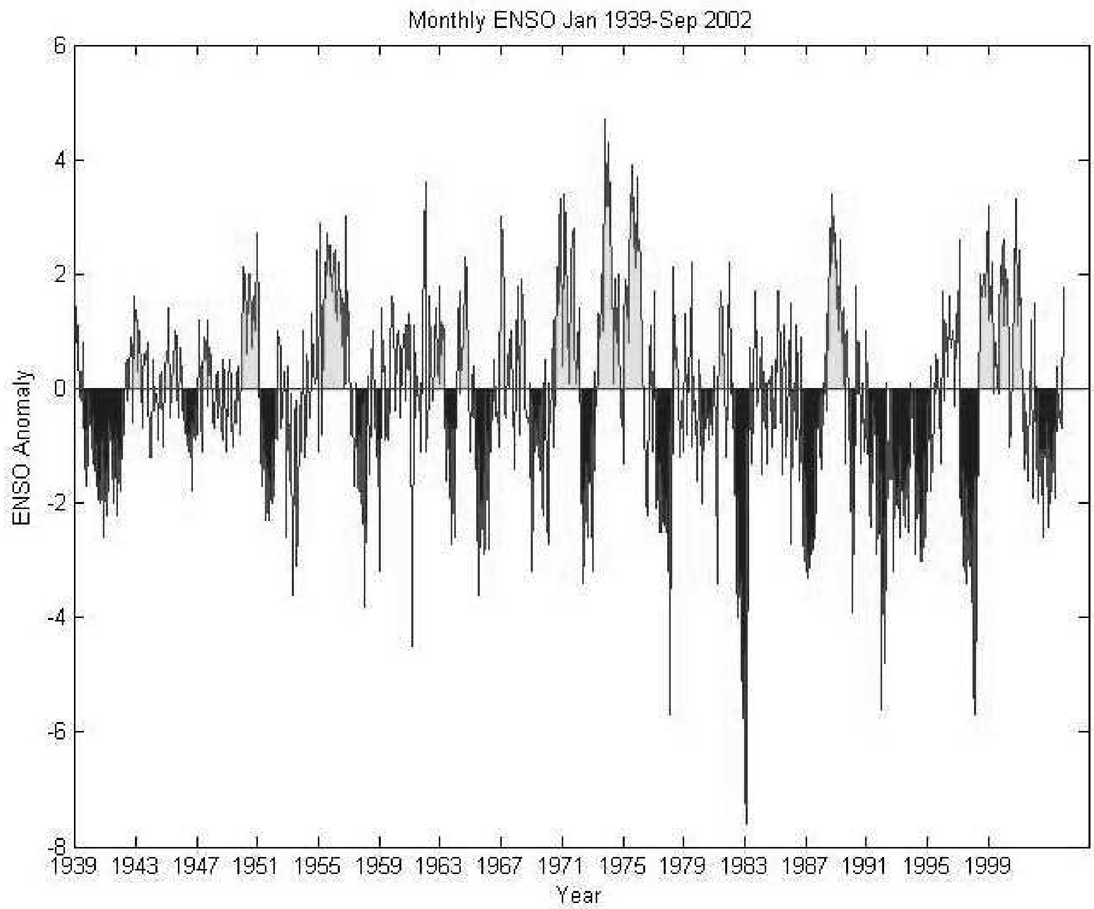

Figure 5. Fluctuations in ENSO captured by the SOI index. Red represents El Niño, while blue represents La Niña. (from Wyckoff, 2005).

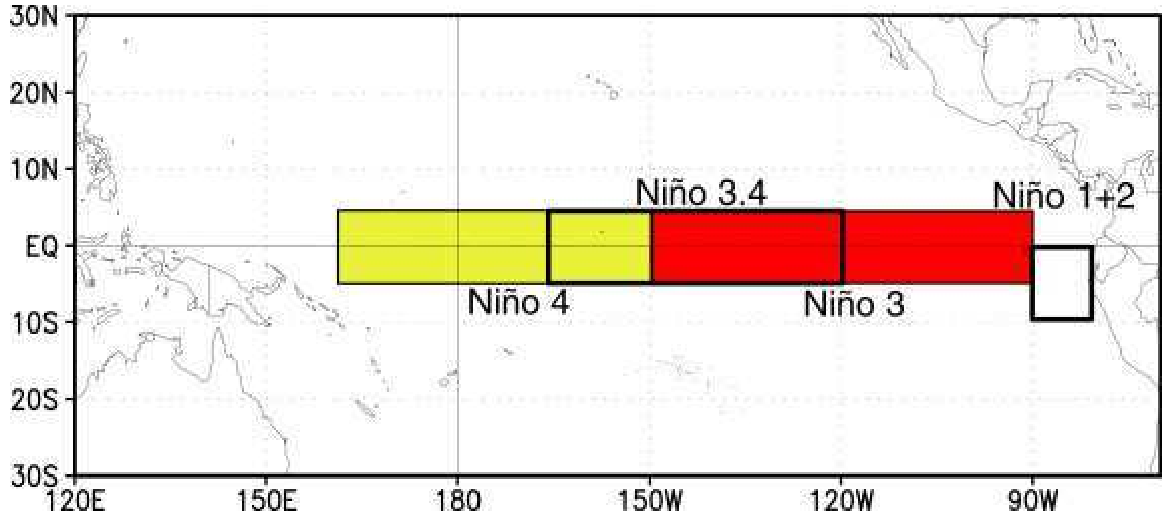

Figure 6. A graphical depiction of the four Niño regions defined by the Climate Analysis Center (CAC; Now known as the Climate Prediction Center) (from http://www.cpc.noaa.gov/products/analysis_monitoring/ensostuff/ninoareas_c.jpg).

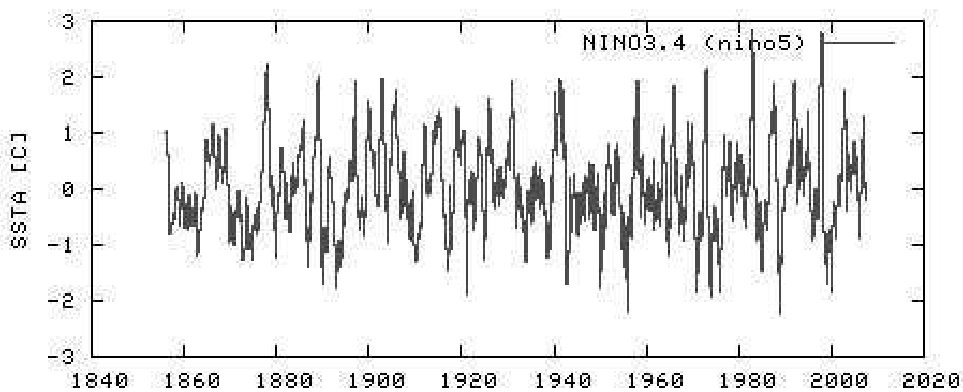

Figure 7. The El Niño3.4 Index displaying SST anomalies (from http://climexp.knmi.nl/getindices.cgi?NCEPData/nino5+NINO3.4+i+someone@somewhere).

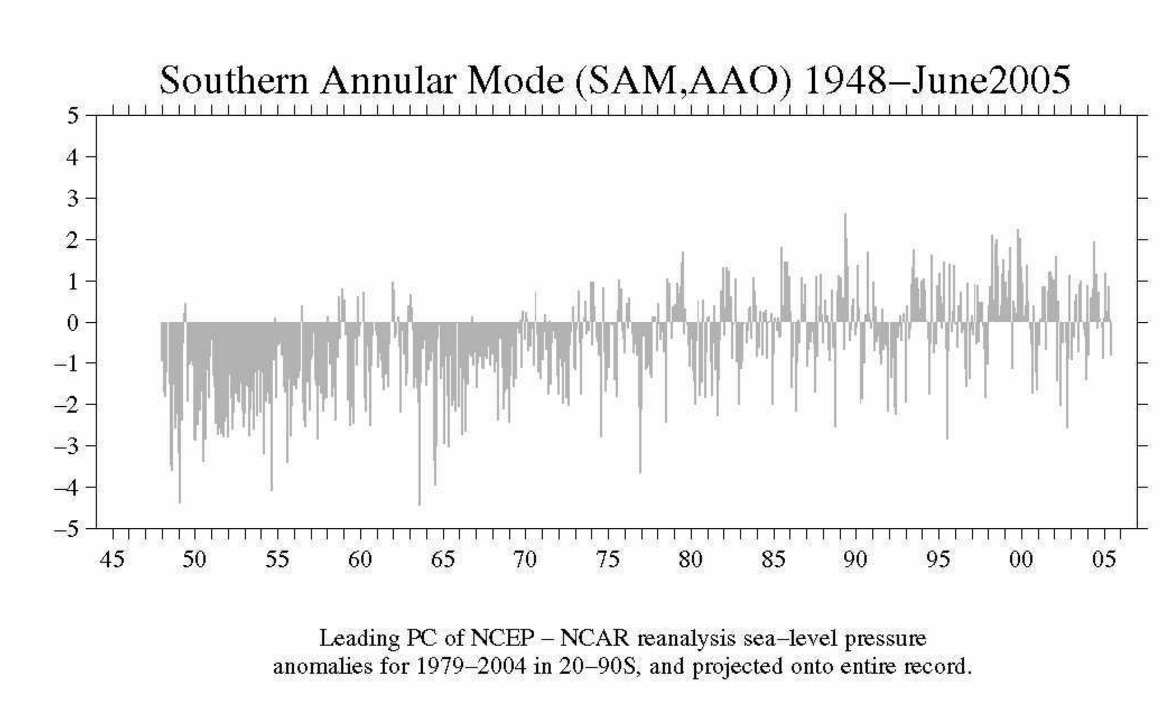

Figure 8. A time series of the Antarctic Oscillation from 1948 to June 2005. (from Todd Mitchell, http://jisao.washington.edu/aao/slp/samslpreanalysis19482005.png)

4. Cloud Mass Transport

The focus on this study is the relationship between cloud mass transport (CMT) events and weather and climate of the Antarctic. Time animations of the Antarctic composite satellite images reveal evidence of these CMT events. A clear cut definition of a CMT event is formulated, as well as a method to accurately track and count individual events.

4.1 Cloud Mass Transport Defined

Cloud mass transport (CMT) is defined as an event in which a large, synoptic scale cloud mass travels from an oceanic region perpendicularly onto the Antarctic continent. CMT events are poleward propagating mass of clouds, transported onto the continent of Antarctica in a pre-defined region for a period of at least two days. Events less than a period of 48 consecutive hours were not considered and not counted as relevant to this research. CMT events which carried over to a new month or new year were considered one event, and the number of days per each month was recorded, allowing some months to obtain a one for the final number of occurrences per a month if no other CMT events occurred during that month. For instance, if a CMT event goes from February 26 through March 1 of 1995, and there are no other CMT events in March of 1995, it would be possible for March 1995 to have a CMT event count of 1, since there was one CMT event that lasted one day in March. The time period covered in this study was between November 1, 1992 and October 31, 2002.

If a CMT event lasted a period of time which included partial days, the dates recorded for the event consisted of the days which had the largest duration of CMT. These issues would arise during the start and ending day of CMT events. For example, consider a CMT event that lasted through two synoptic hours on day one, eight on days two and three, and six on day four. The entire length of the CMT event is three full days, but it occurred over a four-day period. This event would be recorded as a three-day event lasting from days two through four.

4.2 Cloud Mass Transport Methodology

Cloud Mass Transport events were obtained by first viewing the Antarctic Composite video at several different animation speeds in both the forward and backward directions. This allowed attention to be focused on any specific areas or sectors for collection and analysis. The viewing of the tape brought primary attention to the four sectors currently focused on in this research. Next, the tape was reviewed several more times, focusing on a different sector of Antarctica each time to identify any cloud transport present in the specific sector or area. Once a transport event was identified, the section of the tape was reviewed several times to obtain the correct length of time of the event- see Figure 9. The CMT events were eye-counted for each sector. The initial tape run for data collection was done twice to check for consistency. Throughout the duration of the second run, the data from the first run was kept separate and never referenced to ensure no bias would be made. The data was tallied according to each month within the four different sectors. A record of the specific days per month was also recorded.

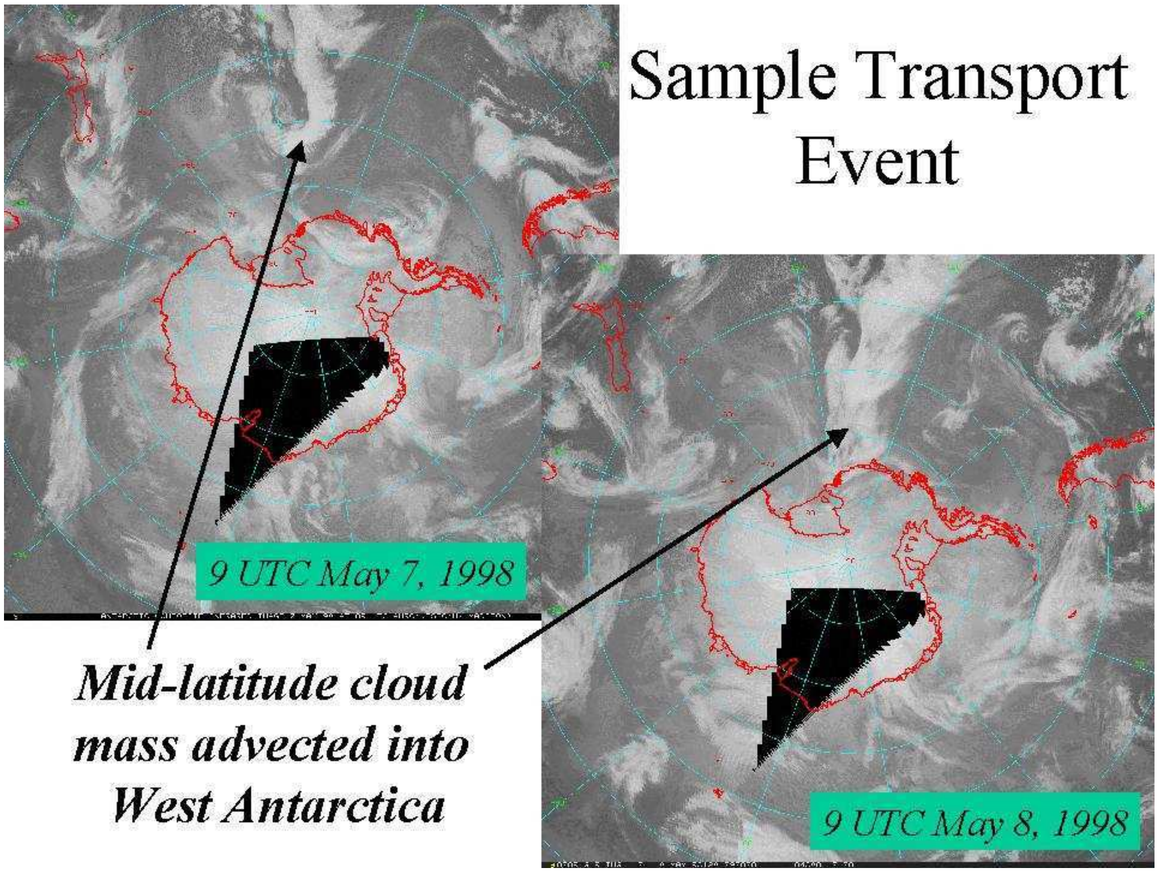

Figure 9. A satellite composite of a cloud mass transport event on 7-8 May, 1998.

5. Results

CMT events were counted by viewing the ten years of satellite composite imagery and were binned on a monthly basis for each sector. Statistical analyses were performed on the data, including calculation of correlation coefficients between the CMT distribution and several climate indices. Student-t tests were used to evaluate significance.

5.1 Data Analysis

5.1.1 CMT Analysis

Prior to the start of this study, it had been noticed by Stearns and Lazzara that there were several geographic regions had frequent and consistent CMT activity, particularly regions of West Antarctica (Stearns and Lazzara, pers. comm., 2001). CMT events were observed in four dominant locations in Antarctica; Marie Byrd Land, Ellsworth Land, Enderby Land, and the Queen Mary Coast (Figure 10). The locations were noted and longitudinally defined regions prior to the collection of the CMT events. Table 2 shows the longitude values for the initial sectors.

After preliminary analysis, the initial sector locations were modified to better define the events. The sectors in West Antarctica, Marie Byrd Land and Ellsworth Land, were narrowed down and separated at 100° W to eliminate any interactions between the two sectors, as well as focusing on smaller regions. The 20° refinement of Marie Byrd Land reduced the area to between 110° W and 140° W. Ellsworth Land was tapered down on one end, making the refined sector to be located between 80° W and 100° W. The sectors of Enderby Land and the Queen Mary Coast were not refined, and will not be discussed in further detail.

For each sector, the 10 year dataset of CMT events was analyzed in various ways. Plots were made which compared the average number of CMT events per year and per month. The analysis of these plots focused on determining any relationship between the two near-adjacent sectors.

5.1.2 Climatological Analysis

Once the CMT events were recorded for Marie Byrd Land and Ellsworth Land, the totals were normalized by month and the results were tabulated and used to calculate a correlation coefficient:

$$r = \frac{1}{n-1} \frac{\sum\left((X_n - X_0)(Y_n - Y_0)\right)}{\sqrt{\left(\sum (X_n - X_0)^2 \sum (Y_n - Y_0)^2\right)}} \qquad (1)$$

where X_n is a specific data value from data set #1, X_0 is the average of data set #1, Y_n is a specific data value from data set #2, and Y_0 is the average of data set #2. In each case, data set #1 is the CMT events from a sector, and data set #2 is one of the three climate indices: the Southern Oscillation Index (SOI), the Niño-3.4 Index, and the Antarctic Oscillation (AAO).

Two different lags were calculated with a lag span of one to thirteen months. The positive (forward) lag represents the climate index lagging the CMT, while the negative (reverse) lag represents the CMT lagging the climate index. Both lags were calculated for each climate index. Once the lags were calculated, plots were created comparing CMT and the climate index for each of the 25 different lags. After each set of lags for each climate index was created, the plots were examined for significant changes and relationships. Then, the correlation values for each lag month were compared to each other in order to search for the best relationship between the CMT and climate index.

Student-t tests were also done for each sector to determine if the correlation of the CMT and each climate index are significant. The data used was from the zero lag correlation coefficient calculations. The equation for the student-t test is as follows:

$$t = \frac{\overline{X}_1 - \overline{X}_2}{s_{\overline{X}_1 - \overline{X}_2}} \text{ where } s_{\overline{X}_1 - \overline{X}_2} = \sqrt{\frac{s_1^2 + s_2^2}{n}} \tag{2}$$

where s is the grand standard deviation, 1 = group one, 2 = group 2, and the denominator is the standard error of the difference between the two means. In each test, group one values represent CMT, and group two values represent one of the climate indices. A p-value, otherwise known as the significance level, was obtained for each combination of CMT and climate index for each of the two sectors. A p-value of less than or equal to 0.05 was considered to be statistically significant. The p-values were calculated using two different programs from two different sources, to check for consistency and accuracy of the programs. They can be found at the following websites: http://www.physics.csbsju.edu/stats/t-test_bulk_form.html and http://www.graphpad.com/quickcalcs/ttest1.cfm?Format=C.

5.1.3 Case Studies

Three case studies were examined in Marie Byrd Land, spanning times from June 4-13, 1997, September 7-12, 1999, and February 10-12, 2000. AWS data from six stations in the Marie Byrd Land region were collected and analyzed. If available, air temperature, relative humidity, pressure, wind speed and wind direction were gathered from each station.

The six stations and their latitude, longitude, and elevation are listed in Table 3. Refer to Figure 1 for a map of all six stations. All six stations were operational for all or some aspects of the case studies. Byrd Station and Mount Siple sites did not have the equipment to measure relative humidity for any of the case studies. Additionally, Byrd Station stopped transmitting for a period starting in May 1999, resulting in no data transmitted for the September 1999 case study, and also had problems in 2000 with wind data, which were removed. The Mount Siple site did not have an aerovane for measuring wind speed and wind direction for any of the case studies. Erin site had a non-functioning aerovane in 1997, and stopped transmission for a period including the September 1999 case study. Elizabeth site also stopped transmission for a period which included the September 1999 case study. Harry site stopped functioning in 1997, until a new station was installed in 1999. Swithinbank site was the only site that was completely operational during all three case studies.

Daily mean composites were created for several meteorological variables using National Centers for Environmental Prediction Center/National Center for Atmospheric Research (NCEP/NCAR) reanalysis data. The program used to create the composites can be found at the following website: http://www.cdc.noaa.gov/Composites/Day/. The following variables were computed for each case study at 500 hPa – Geopotential Height, Vector Wind, Relative Humidity, and Precipitable Water. The data was plotted in a Southern Hemisphere Polar Stereograph projection, displaying the area between -50° and -90° latitude.

5.2 Results

The 10 year dataset of CMT events has provided interesting results with respect to the climate indices, as well as valuable information on the relationship of CMT events between the two sectors. In particular, the SOI proved to have the most interesting and valuable results out of all the climate indices. The case studies are particularly useful in correlating meteorological data with CMT events.

5.2.1 CMT Results

The CMT events were examined to look for patterns and relationships between the two sectors. The average number of CMT events per year was examined for both sectors. Marie Byrd Land and Ellsworth Land both showed similar results in having the highest number of events per year in 2002 (Figure 11 and Figure 12). Additionally, each sector had another peak. Marie Byrd Land also had a peak in 1997, while Ellsworth Land had a peak in 1998 (1997-1998 was considered a strong El Niño year).

The average number of CMT events per month was also examined for the 10 year period. Marie Byrd Land had a large peak in June, while Ellsworth Land had a peak in September, indicating a shift in the peak month of CMT events between the two sectors (Figure 13 and Figure 14). Another analysis of CMT events looked at the length of every CMT event which transpired over the 10 year period. The analysis shows the majority of the CMT events in both sectors occurred for a period of two to three days, with over 75 percent of CMT events having a length of five or less days (Figure 15). Additionally, Ellsworth Land also had more CMT events (190) than Marie Byrd Land (165).

5.2.2 CMT vs. Climate Indices

Correlation coefficient values were calculated and examined, and the range of values was shown to be fairly small, compared to suggested guidelines of the interpretation of a correlation coefficient. Values obtained ranged from -0.24 to 0.30, which are considered small and medium according to Cohen (1988). Cohen describes small correlations to have negative values between -0.29 to -0.10 and positive values between 0.10 and 0.29, while medium correlations have negative values between -0.49 to -0.30 and positive values between 0.30 and 0.49. The highest correlation values were found to be correlated with the two ENSO indices – the SOI and the Niño-3.4 index, while the AAO produced no significant correlation.

The one month reverse lag of Marie Byrd Land has the highest negative correlation, as well as overall correlation of CMT with the SOI at a value of -0.24 (Figure 16). Overall, negative correlation values dominate the different lag correlations between -13 and +13 months, with fairly small values for the correlations (Figure 17). Additionally, between lag months 0 and positive 13, there is a shift from negative correlation values from lag months 0 to 6, to positive correlation values from lag months 7 to 13. An indication of a phase change is present as the shift from negative to positive occurs between lag months six and seven.

Ellsworth Land has the highest positive correlation value of CMT with the SOI of 0.20 at the five month positive lag. The plot of CMT and SOI shows a similar pattern in the positive and negative correlations for several groups of days. However, Ellsworth Land is opposite of what is seen in Marie Byrd Land, as there are more positive correlations than negative ones (Figure 18). The average value of the correlations for both lags is significantly smaller than those of Marie Byrd Land, and mainly positive throughout all lags (Figure 19). The magnitude of all of the negative lag correlations are equal or less than -0.10. The only clear signal in the lag correlations is the all positive correlation values from the positive 2 to 13 month lags.

The correlation between Marie Byrd Land and Niño-3.4 was the most significant obtained in this study. The zero lag correlation had a value of 0.30, the only value considered to be a medium correlation. The plot of CMT and Niño-3.4 for Marie Byrd Land shows similar signals seen in the previous plots to the positive and negative correlations between the two variables (Figure 20). The lag correlations of CMT from Marie Byrd Land and Niño-3.4 show an interesting relationship in the progression of the lag months away from zero (Figure 21). The zero lag month correlation is the highest positive value, and as both the positive and negative lags progress to +/- 13 months, the correlations decrease, and become the two highest negative values.

The overall results for CMT relationships with the AAO were fairly insignificant. Correlation values for Marie Byrd Land and Ellsworth Land with the AAO fell under +/- 0.20. Additionally, the lag correlations for the AAO in both sectors were examined, and no evidence of a pattern or any features were found (see Appendix).

Student-t tests produced noteworthy results for Marie Byrd Land and Ellsworth Land with the SOI. The p-value for the zero lag of Marie Byrd Land CMT events and the SOI produced a value of 0.050, which is considered to be statistically significant. The zero lag CMT events for Ellsworth Land and the SOI resulted in a not quite statistically significant value of 0.058. Even though the Niño-3.4 index produced the highest correlation coefficient value, it was found to be not statistically significant in both CMT sectors. Figure 22 shows whisker plots created which show the mean of each variable with 1σ error bars and the data swarm. Additionally, the p-values for the zero lag of Marie Byrd Land and Ellsworth Land with the AAO were also considered not statistically significant, with their respective p-values being far away from the threshold of 0.050 (Figure 23).

5.2.3 Case Studies

The pressure, wind speed and relative humidity data from the June 3-14, 1997 case study provided interesting results which might be used to characterize a CMT event. During this time period, several consistent patterns relating to the onset of a cyclone were present in the meteorological data. Pressure levels dropped 18 to 33 hPa from June 3-9, with two significant drops occurring at four stations on the 7th and the 9th (Figure 24). Mount Siple station, at a much lower latitude then the other stations, also showed similar peaks, however they occur a half day to a day earlier. Wind speed and relative humidity plots also show similar changes over the 12 day period. There was an increase in wind speed of an average of 20 m/s throughout the duration of the event, with the most significant changes occurring during the same time as the pressure changes – on the 7th and the 9th (Figure 25). The additional two case studies display similar results, although the changes during the duration of the events are not as prominent, most likely due to the fact that the time period is significantly shorter (see Appendix).

The daily mean composites calculated for each case study using NCEP/NCAR reanalysis data support many of the findings from the AWS data. The 500 hPa geopotential height plot shows an upper level cyclone over the Ross Ice Shelf region in West Antarctica, resulting in the perpendicular flow onto the continent over the Marie Byrd Land region

(Figure 26). Compared to the seasonal mean 500 hPa geopotential heights (Figure 3), the NCEP/NCAR reanalysis data depicts a stronger upper level low, branching out into an almost second center over the center of the continent. Wind vectors at 500 hPa support the geopotential height contours, showing the only perpendicular flow over the continent onto Marie Byrd Land (Figure 27). Relative humidity levels at 500 hPa illustrate a higher level over Ellsworth Land and the Marie Byrd Land-Ellsworth Land boundary than anywhere else on the Antarctic continent. Furthermore, precipitable water levels at 500 hPa are higher over West Antarctica than the rest of the continent. The September 1999 and February 2000 case studies show similar results in the NCEP/NCAR reanalysis data plots. While not as strong, indications of a midlatitude cyclone over the West Antarctic region, with strong flow into the continent over Marie Byrd Land is still present in the data. Refer to Figure 3 for the average winter and spring patterns of geopotential height at 500 hPa.

CMT Sector	Longitudinal Boundary
Marie Byrd Land	100° W - 150° W
Ellsworth Land	70° W - 100° W
Enderby Land	40° E - 60° E
Queen Mary Coast	93° E - 103° E

Table 2. The initial longitudinal boundaries for each of the CMT sectors in Antarctica.

Station Name	Latitude	Longitude	Elevation
Byrd Station	80.01 °S	119.40 °W	1530 m
Elizabeth	82.61 °S	137.08 °W	519 m
Erin	84.90 °S	128.83 °W	990 m
Harry	83.00 °S	121.39 °W	945 m
Mount Siple	73.20 °S	127.05 °W	230 m
Swithinbank	81.20 °S	126.18 °W	959 m

Table 3. A list of the latitude, longitude, and elevation of the six AWS stations used in the case studies.

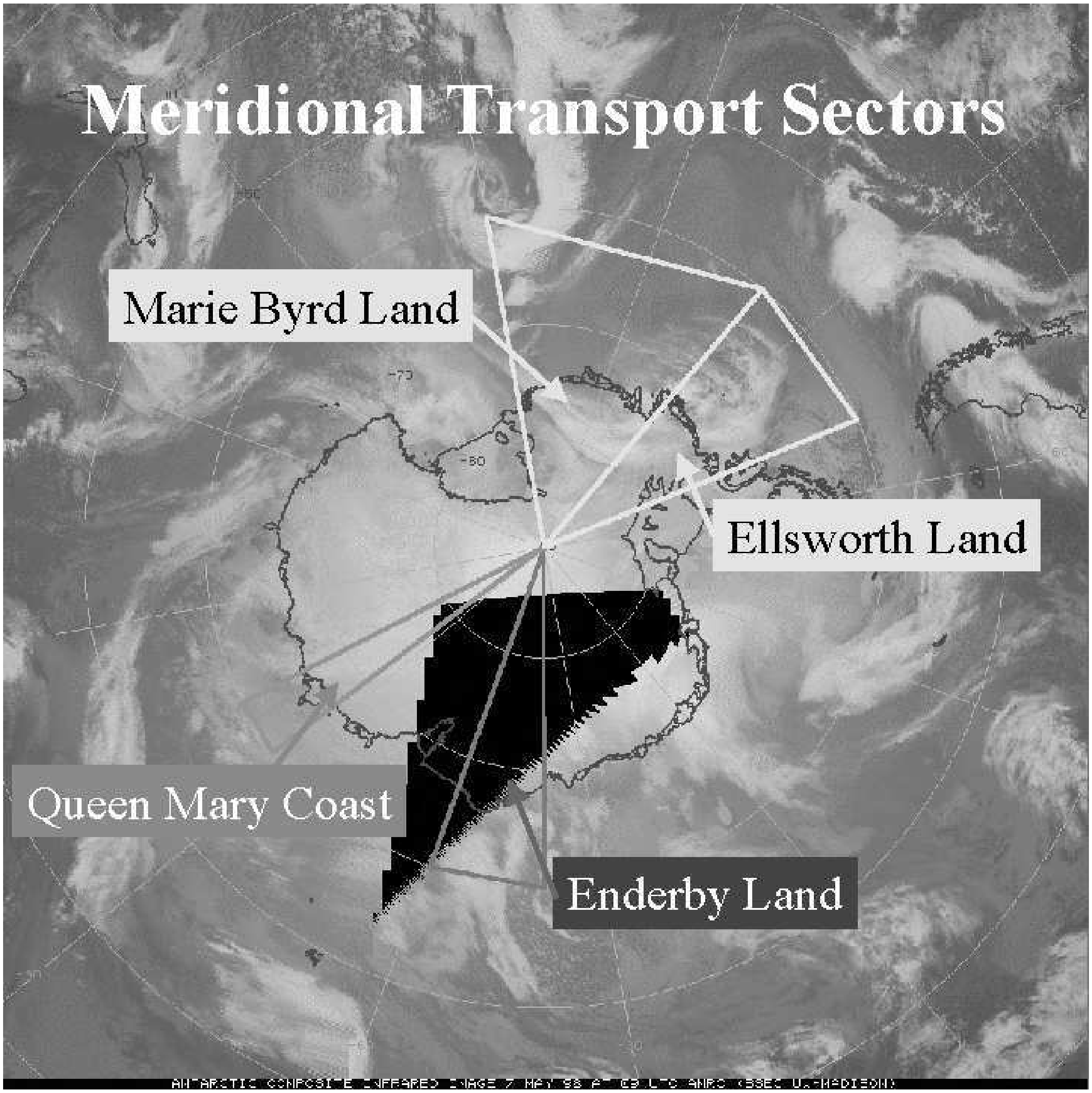

Figure 10. The four dominant sectors of cloud mass transport in Antarctica.

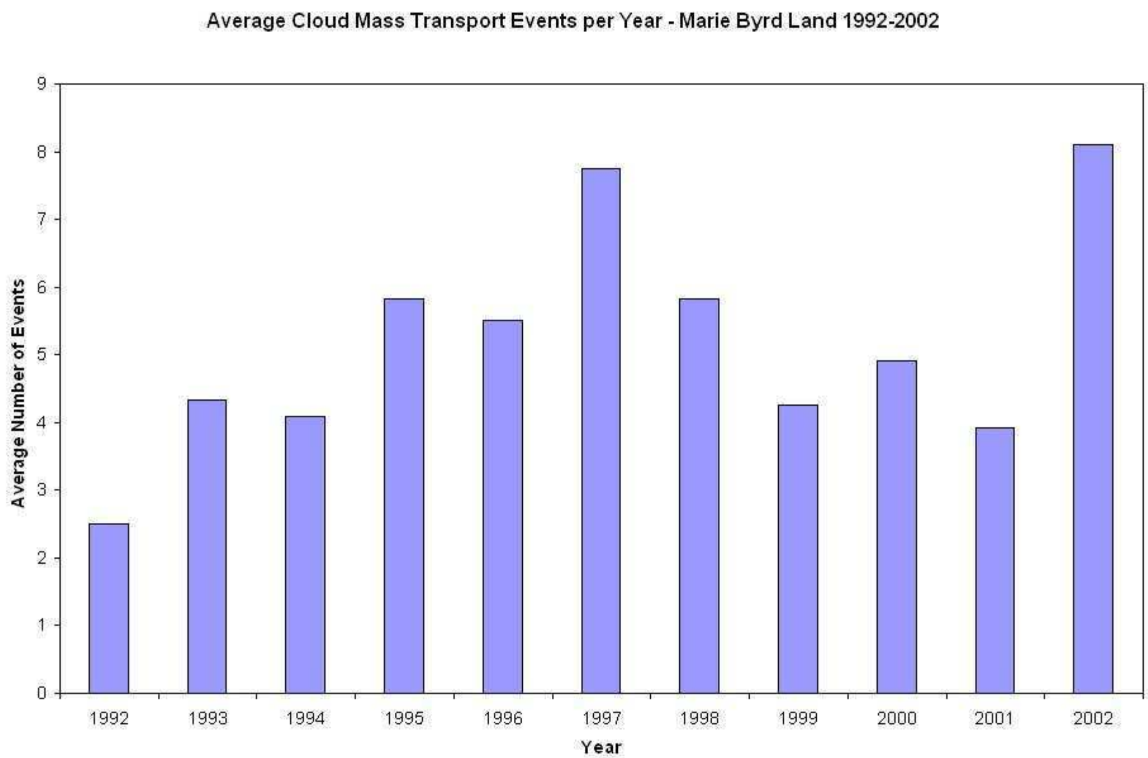

Figure 11. The average number of CMT events per year for Marie Byrd Land for the period 1992-2002.

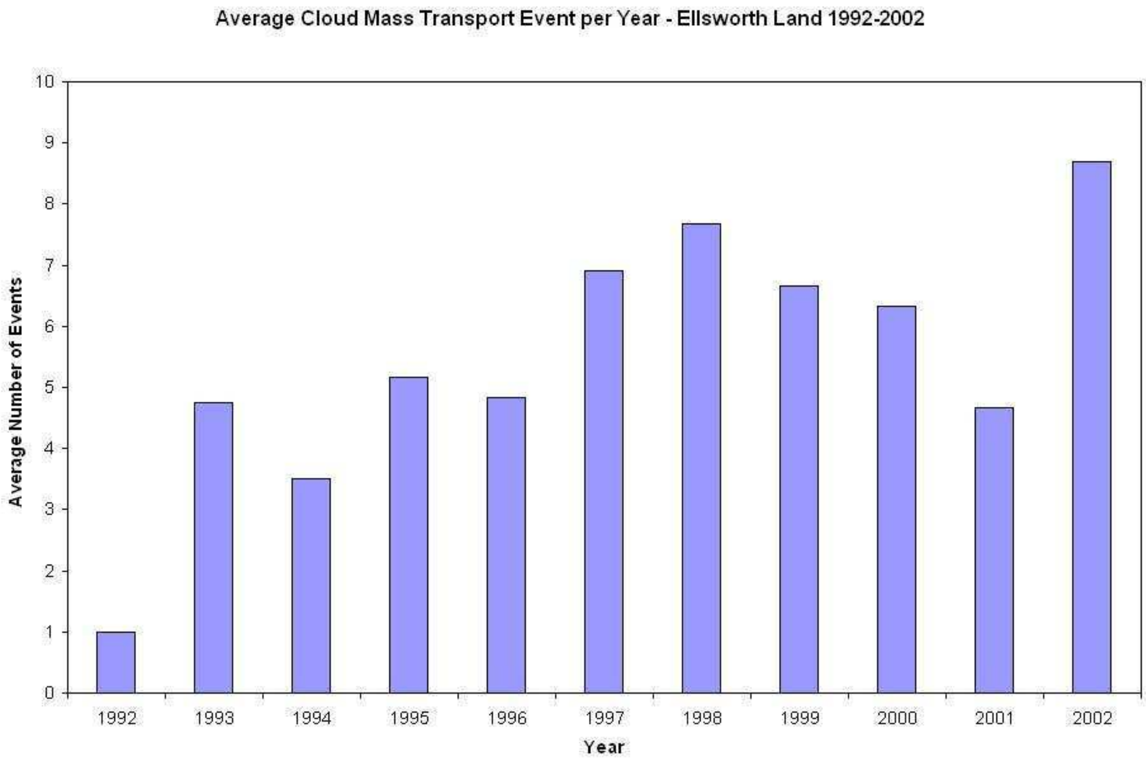

Figure 12. The average number of CMT events per year for Ellsworth Land for the period 1992-2002.

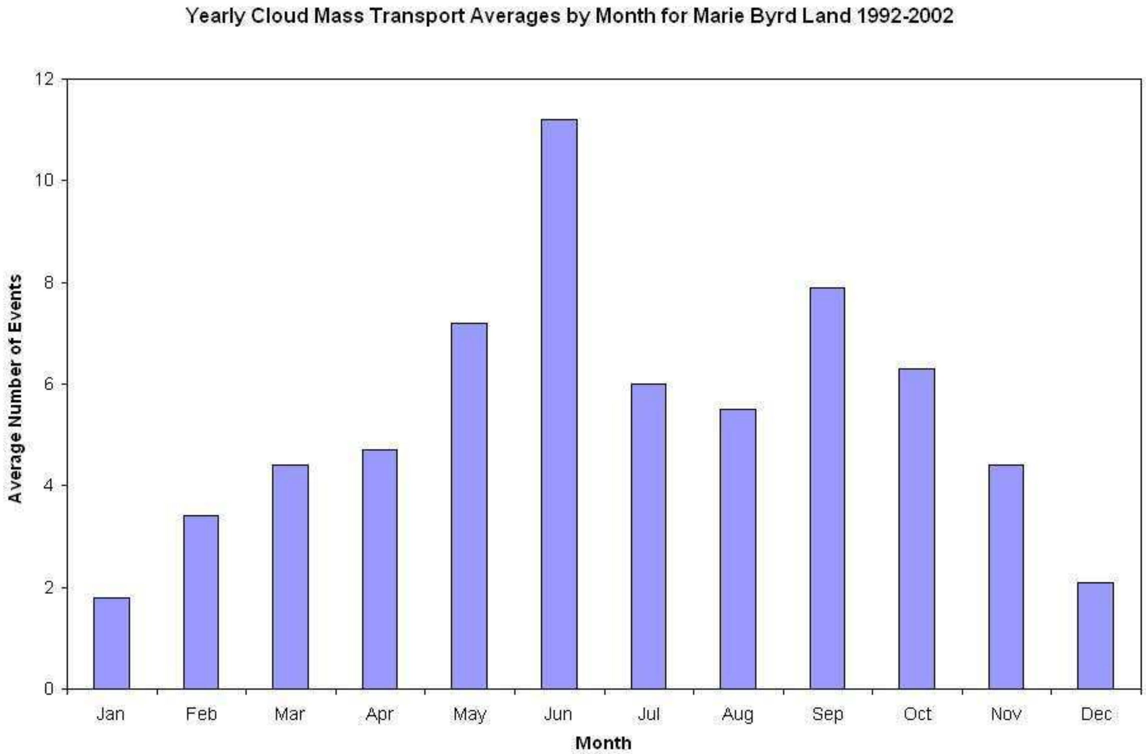

Figure 13. The yearly CMT averages by month for Marie Byrd Land for the period 1992-2002.

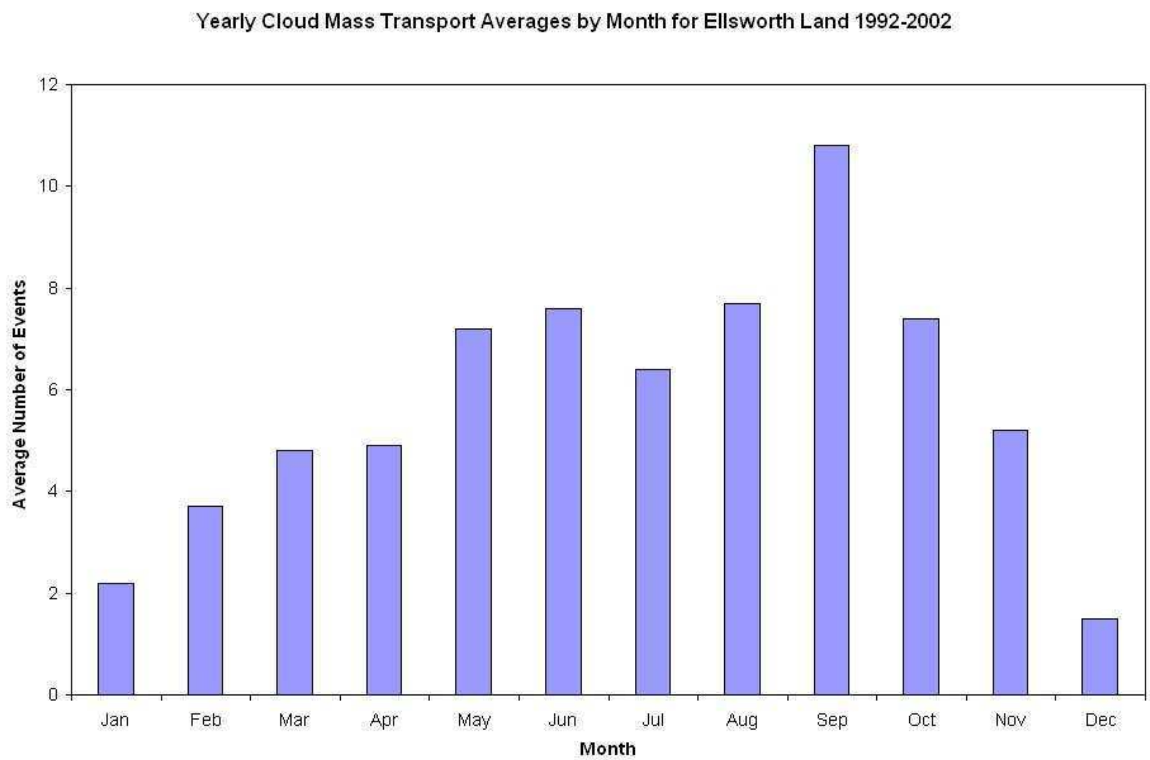

Figure 14. The yearly CMT averages by month for Ellsworth Land for the period 1992-2002.

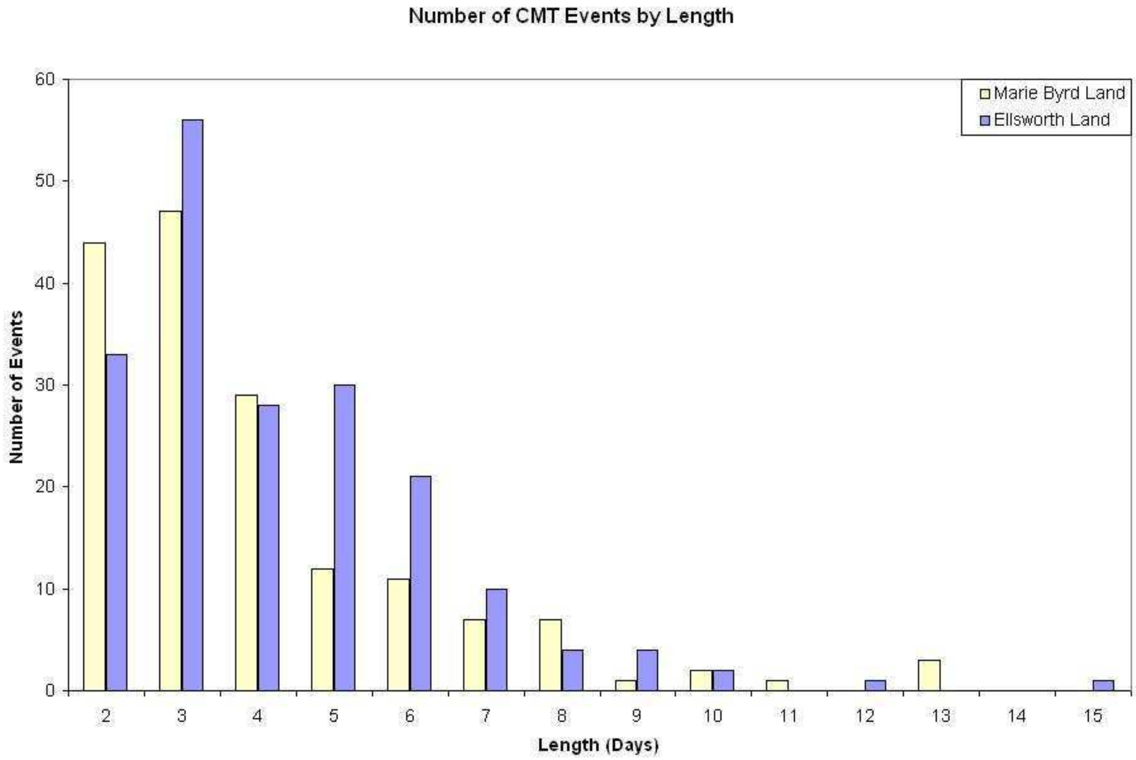

Figure 15. A graph depicting the spread of the length of CMT events for Marie Byrd Land and Ellsworth Land for the period 1992-2002.

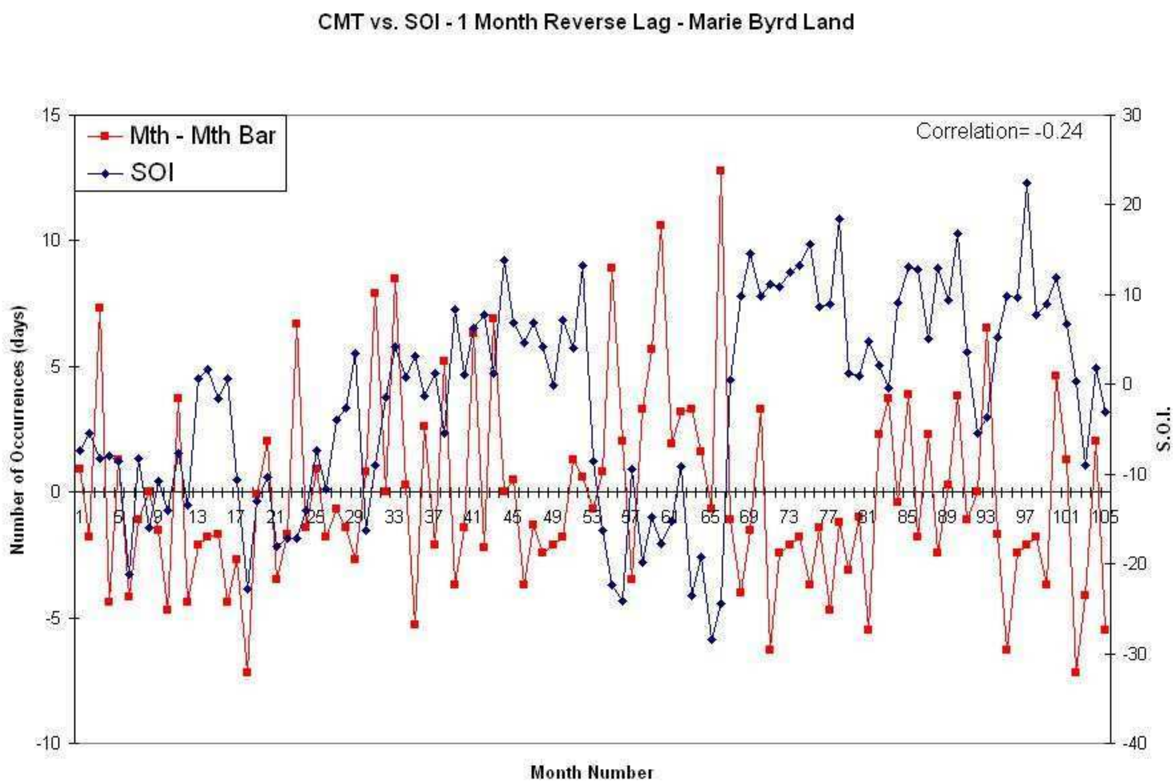

Figure 16. The 1 month reverse lag plot CMT vs. SOI for Marie Byrd Land.

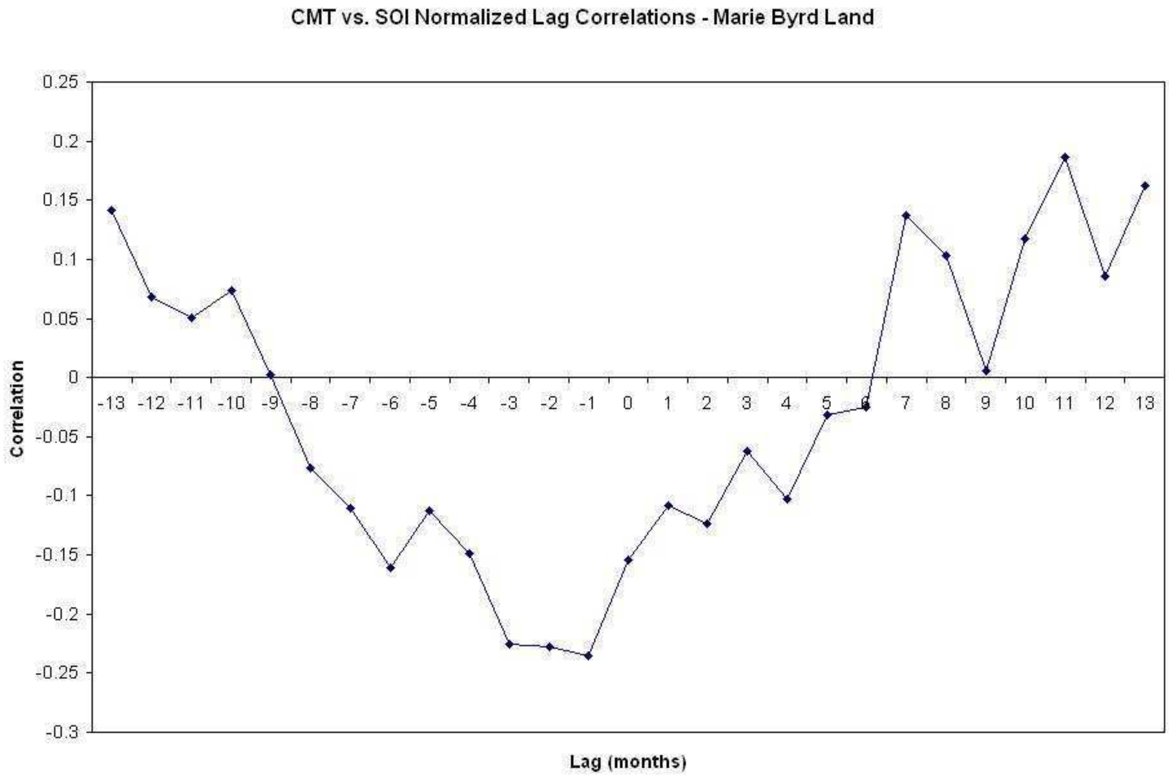

Figure 17. A plot of CMT vs. SOI Lag Correlations for Marie Byrd Land from months -13 to +13.

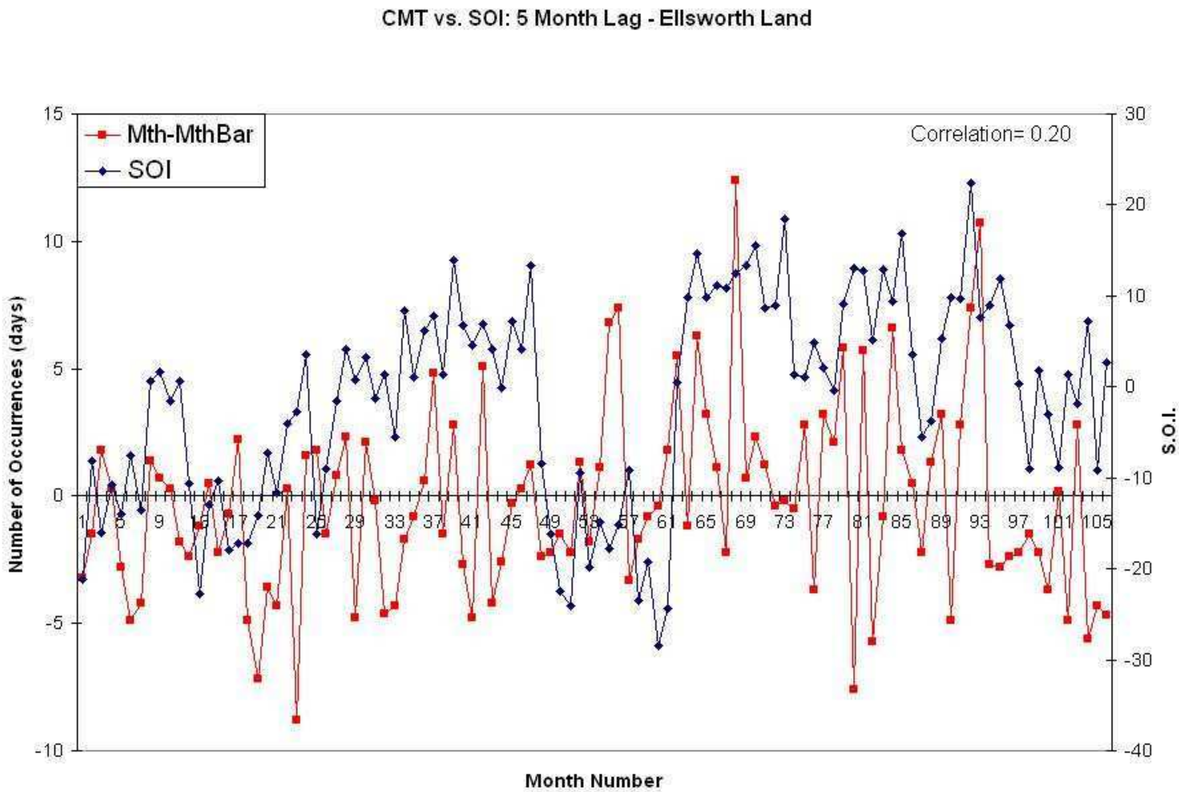

Figure 18. The 5 month lag plot of CMT vs. SOI for Ellsworth Land.

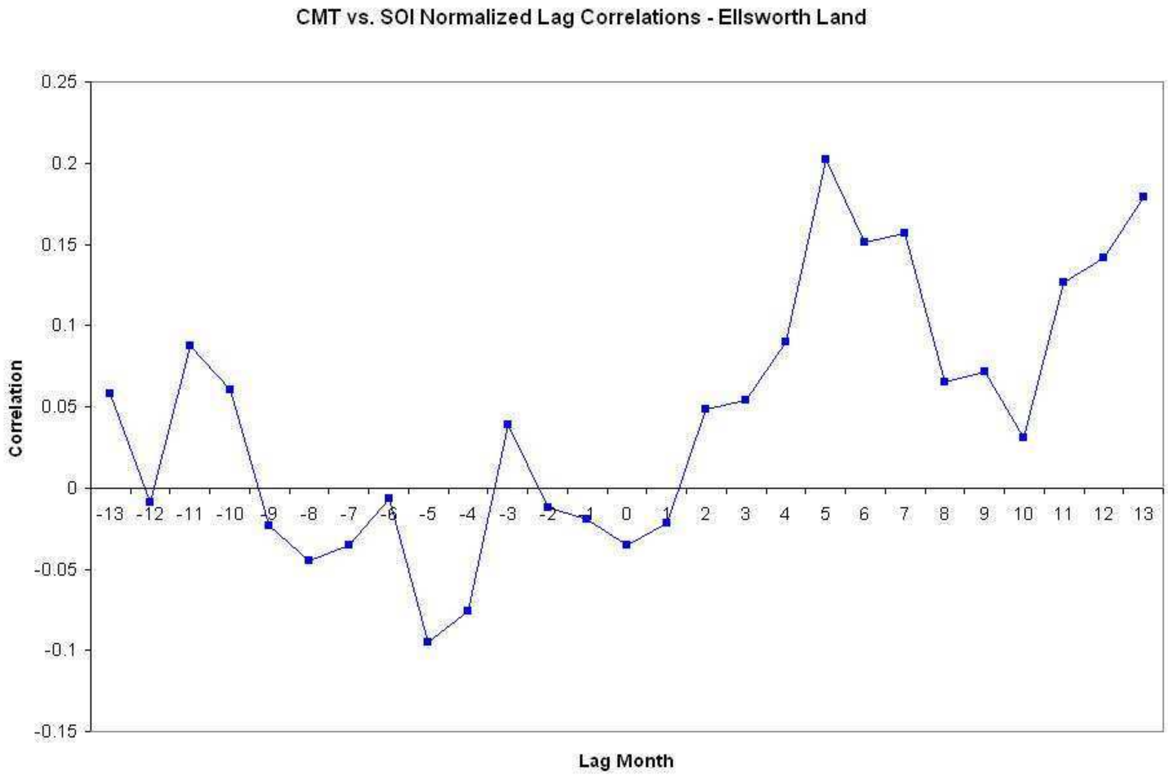

Figure 19. A plot of CMT vs. SOI Lag Correlations for Ellsworth Land from months -13 to +13.

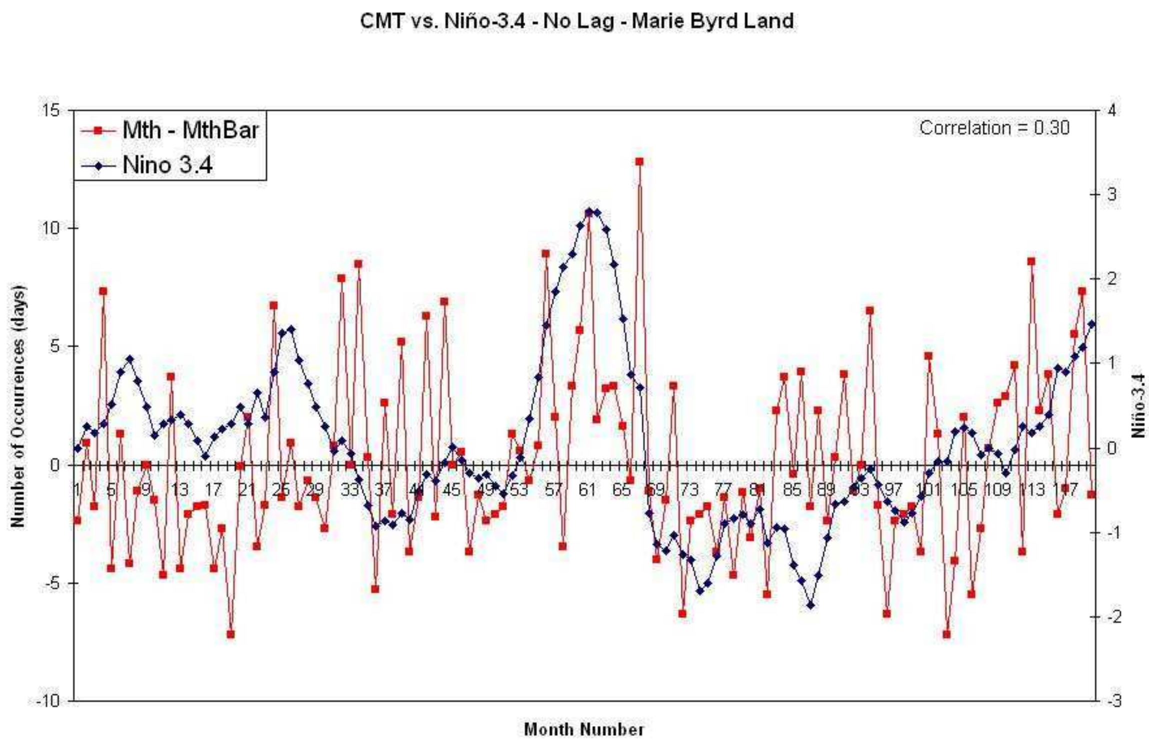

Figure 20. The zero lag plot of CMT vs. Niño-3.4 for Marie Byrd Land.

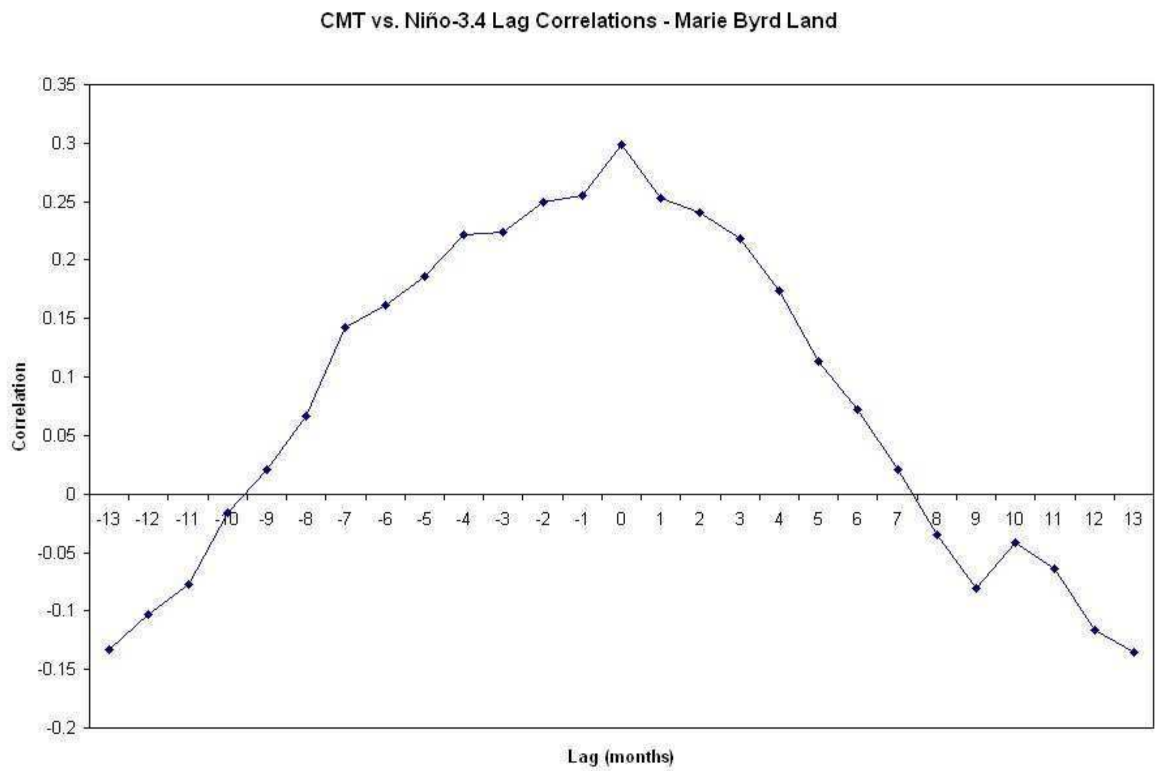

Figure 21. A plot of CMT vs. Niño-3.4 Lag Correlations for Marie Byrd Land from months -13 to +13.

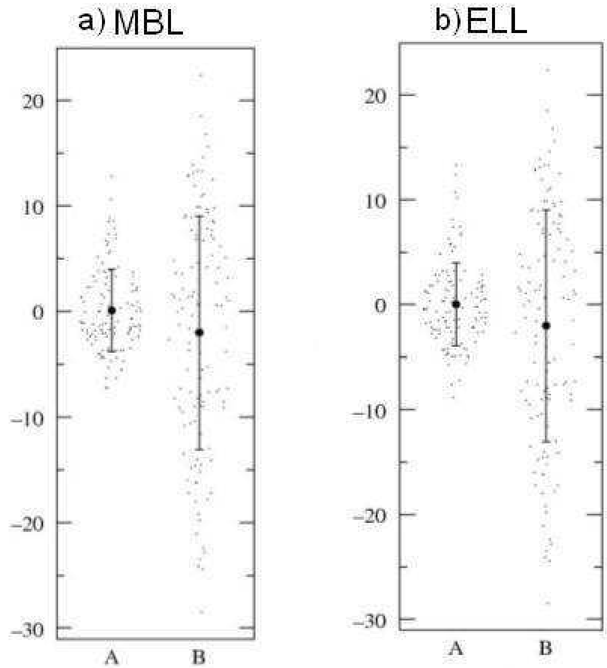

Figure 22. Whisker plots for a) Marie Byrd Land and b) Ellsworth Land. The A whisker plot represents CMT at the respective location and B represents the SOI.

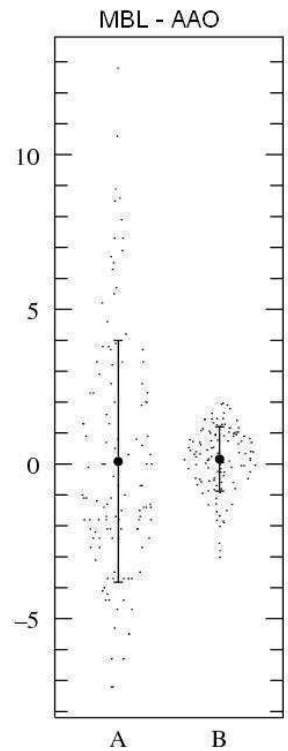

Figure 23. A whisker plot for Marie Byrd Land and the AAO. The A whisker plot represents CMT events and B represents the AAO.

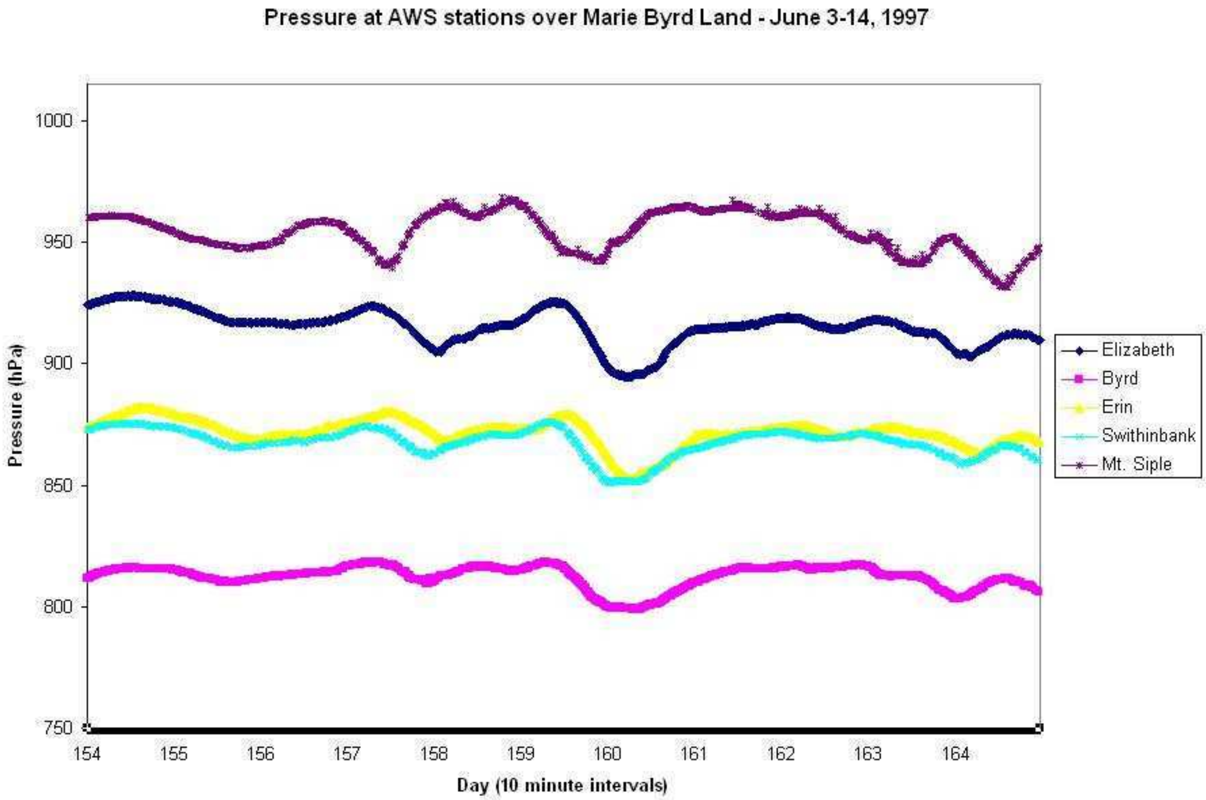

Figure 24. A plot showing pressures at five different AWS stations in Marie Byrd Land from June 3-14, 1997.

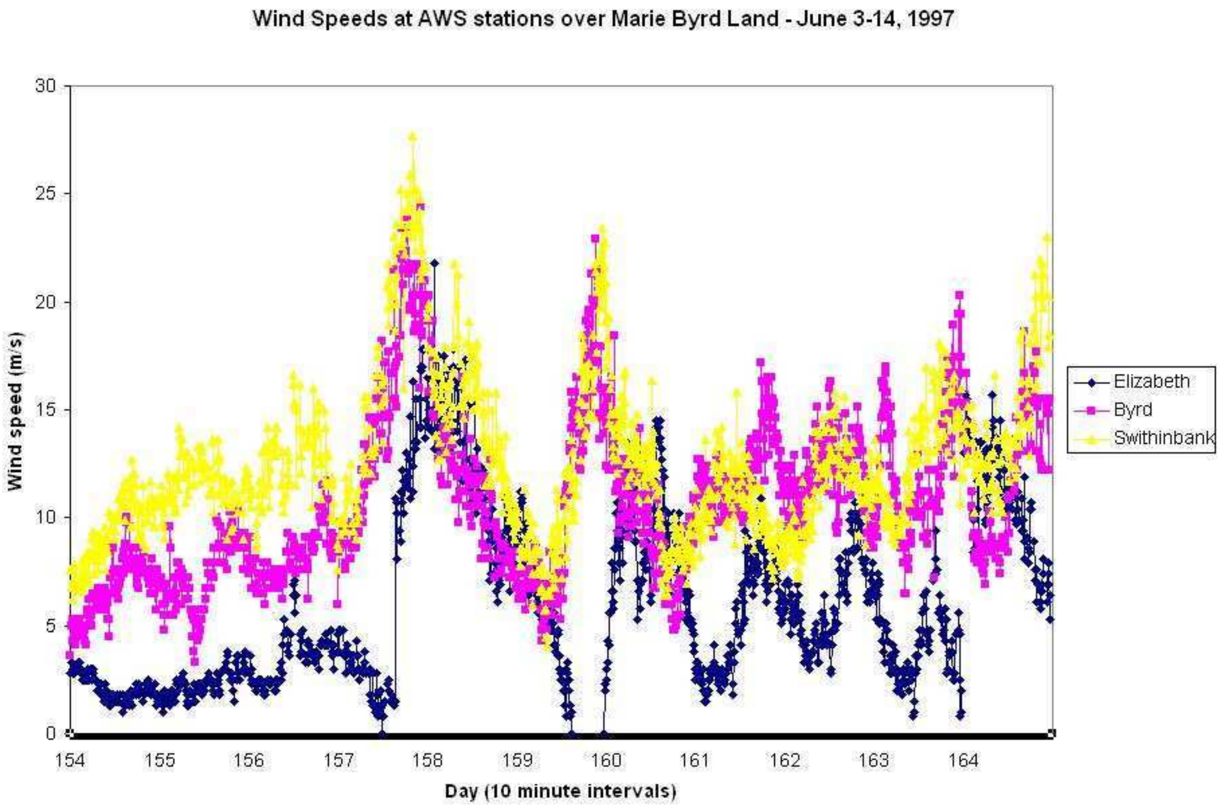

Figure 25. A plot showing wind speeds at three different AWS stations in Marie Byrd Land from June 3-14, 1997.

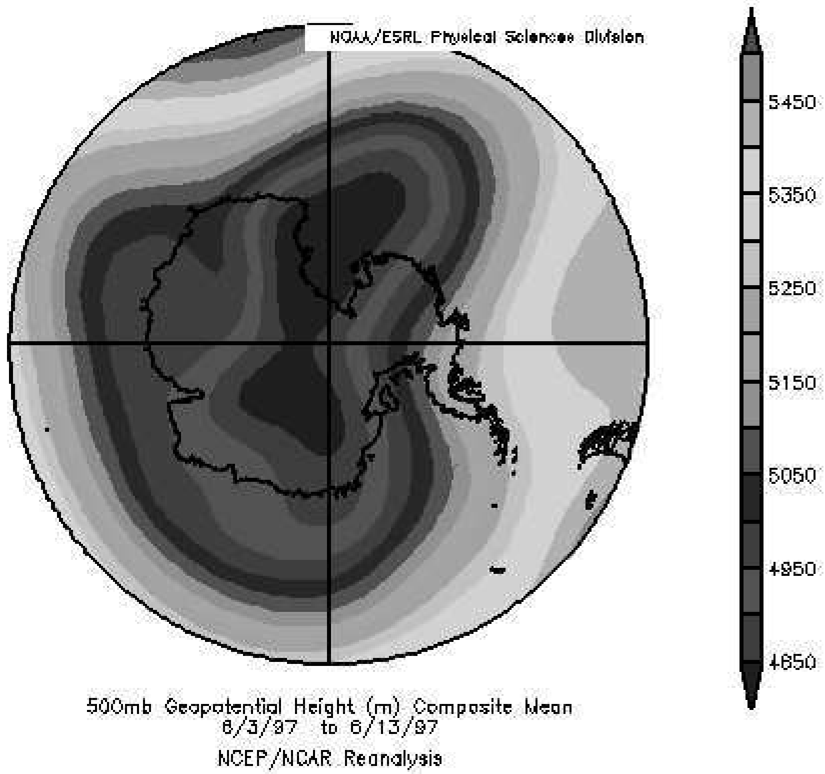

Figure 26. 500 hPa Geopotential heights calculated from daily NCEP/NCAR reanalysis data for the period June 3-14, 1997.

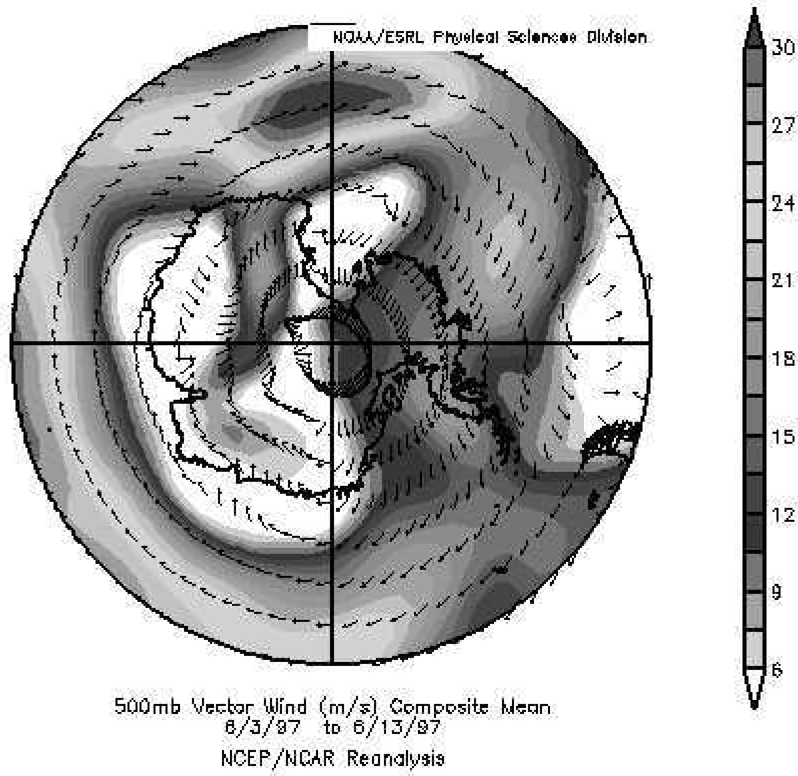

Figure 27. 500 hPa vector winds calculated from daily NCEP/NCAR reanalysis data for the period June 3-14, 1997.

6. Conclusions and Future Work

This section provides preliminary conclusions, as well as plans for future work.

6.1 Conclusions

A prominent result from this study for weather forecasting in Antarctica is the relationship between CMT and ENSO. Average correlation values were found to be the largest out of all the indices examined, including the highest values in the one month reverse lag for Marie Byrd Land and the five month lag for Ellsworth Land. Additionally, student-t tests produced p-values of 0.05 and 0.06 in Marie Byrd Land and Ellsworth Land, respectively, for the zero lag correlations. CMT over West Antarctica showed secondary peaks in 1997 for Marie Byrd Land and 1998 for Ellsworth Land; 1997-1998 was a strong El Niño year, and could possibly explain the cause behind the peaks. With the six month shift between the largest correlation values for each sector moving from Marie Byrd Land to Ellsworth Land, the number of CMT could have been affected as the El Niño event progressed into 1998, causing the peak shift. 2002 was also the start of an El Niño year, and CMT events in both sectors increased for that year, so it is quite possible for the same pattern to become evident with additional data.

The highest correlation coefficient obtained was from CMT events in Marie Byrd Land with the Niño-3.4 index at a zero month lag, although student t-test results proved this correlation to be not statistically significant. However, the fact that the highest correlation value was received with the zero month lag could indicate that the increase in CMT events at Marie Byrd Land may be associated with the onset of an El Niño event. Differences between the formulation of the SOI and the Niño-3.4 may have resulted in the differences in the lag months of the peak correlation values, as the SOI is calculated with surface pressure differences, and the Niño-3.4 is calculated with sea surface temperatures (SSTs). The results from the SOI and Niño-3.4 indices support other studies done on relationships between ENSO and features of Antarctica, such as the study by Smith and Stearns (1993).

The prominent cyclonic activity found in West Antarctica by Jones and Simmonds (1993) is similar to the findings of this study because the main sectors of activity occur in similar locations. Many of the cyclones in the area may be directly related with CMT events. The difference in the peaks of CMT events per month between the two sectors suggests a delayed pattern. A peak in Marie Byrd Land happens in June, while the peak in Ellsworth Land occurs in September. It is possible that the shift in the CMT events can be explained by another process; however, it is clear that the best times of the year to avoid CMT events in West Antarctica are the peak summer months in December and January. There seems to be no apparent relationship with the AAO, as the climate index produced poor results in both the correlation coefficients as well as the student-t tests.

The AWS case studies proved useful in verifying the extent of the CMT events with supporting surface observations. That the CMT events were originally obtained by visual methods could lead to skepticism if they are not validated. The lack of multiple types of long-lived, continuous AWS data in West Antarctica is clearly an issue shown by the results of the case studies, as the pressure records clearly provided the most significant contribution. One major problem is that case studies in Ellsworth Land were not able to be performed because there were no operating stations over the area during the 10 year time period of the study. While six stations were used in the Marie Byrd Land case studies, only one was along the coast line as well as below 70 degrees South. Also, since not every station was equipped with working wind and relative humidity equipment, it was difficult to draw strong relationships without this important data.

The validation of NCEP/NCAR reanalysis data is fairly successful. The results of the AWS case study data compared to the results of the reanalysis daily composite means presented a fairly accurate representation of the overall situation in West Antarctica during CMT events. The most significant variables of note, the 500 hPa geopotential heights, and the 500 hPa vector winds, show a clear-cut depiction of the events, indicating future use of NCEP/NCAR reanalysis data will be beneficial to future studies.

6.2 Future Work

Additional work is needed to determine the extent CMT events have on the weather in West Antarctica. In the immediate future, the extension of the CMT dataset will be a valuable asset, as it is quite possible the current dataset is not long enough to show relationships with the climate signals examine in this study. After November 1, 2007, a 15 year dataset of composites will exist. The addition of 2003 will be beneficial to continuing studies on the relationship between CMT and ENO, as it is a year with a moderate El Niño year, which would add an additional El Niño year to the dataset.

Another analysis option considered for the future is to separate the CMT events based upon the current El Niño state and examine the results of a comparative study between ENSO and non-ENSO years. A further aim is to investigate possible trends from other climate signals. The relationships between other ENSO indices, the semi-annual oscillation and the South Pacific American Pattern, have been considered for further research. Another approach to examining the CMT events is to look at seasonal oscillations.

The development of an automated cloud masking program would be beneficial to the collection of future CMT events. However, the fact that the composites used in this study are only from the 11.0 μm channel would make it difficult to accurately obtain cloud detection results. Visible composites are not a feasible option in this study because part of the area is totally dark for about six months of the year. Satellites play an increasingly important role in research and forecasting over the continent. The launch of new satellites with coverage over Antarctica is necessary to maintain the benefits of new and improved satellite technology. A pole sitter satellite over the South Pole would provide temporal coverage of the region, giving a new view on polar processes (Lazzara, 2005). It is also clear that the installation of several AWS units in West Antarctica, particularly in the region of Ellsworth Land would be beneficial for use in future case studies.

Antarctic Cloud Mass Transport is an important aspect of the Antarctic climate – the interaction between weather events and seasonal/annual signals. Once a strong correlation is found, it will lead to a better understanding of the relationship between CMT events and climate. Further improvements in operational forecasting over West Antarctica will be possible, aiding advancement of Antarctic research.

7. References

Ackerman, Steven A. and John A. Knox, 2003: *Meteorology: Understanding the Atmosphere*. Thompson Learning, Inc., 486 pp.

Arrigo, K. R., G. L. van Dijken, D. G. Ainley, M. A. Fahnestock, and T. Markus, 2002: Ecological impact of a large Antarctic iceberg, *Geophys. Res. Lett.*, **29(7)**, 1104, doi:10.1029/2001GL014160.

Barnston, A. G., and M. Chelliah, 1997: Documentation of a highly ENSO-related SST region in the equatorial Pacific. *Atmos.– Ocean,* **35,** 367–383.

Carrasco, J.F., D.H. Bromwich, and A.J. Monaghan, 2003: Distribution and Characteristics of Mesoscale Cyclones in the Antarctic: Ross Sea Eastward to the Weddell Sea. *Mon. Wea. Rev.,* **131**, 289-301.

Chen, W. Y., 1982: Assessment of Southern Oscillation sea level pressure indices. *Mon. Wea. Rev.,* **110**, 800-807.

Cohen, J., 1988: *Statistical power analysis for the behavioral sciences* (2nd ed.) Hillsdale, NJ, Lawrence Erlbaum Associates. 572 pp.

Godin, R. H., 1977: An investigation of synoptic and associated mesoscale patterns leading to significant weather days at McMurdo station, Antarctica. M.S. thesis, Department of Meteorology, Naval Postgraduate School, 114 pp. [NTIS ADA046247.]

Gong, Daoyi and Shaowu Wang, 1999: Definition of the Antarctic Oscillation Index. *Geophys. Res. Let.*, **4**, 459-462.

Hanley, D.E., M.A. Bourassa, J.J. O'Brien, S.R. Smith, and E.R. Spade, 2003: A quantitative evaluation of ENSO indices. *J. Climate*, **16(8)**, 1249-1258.

Jones, D. A., and I. Simmonds, 1993: A climatology of Southern Hemisphere extratropical cyclones. *Climate Dyn.,* **9,** 131–145.

Kalnay, E., M. Kanamitsu, R. Kistler, W. Collins, D. Deaven, L. Gandin, M. Iredell, S. Saha, G. White, J. Woollen, Y. Zhu, A. Leetmaa, B. Reynolds, M. Chelliah, W. Ebisuzaki, W. Higgins, J. Janowiak, K. Mo, C. Ropelewski, J. Wang, R. Jenne, and D. Joseph, 1996: The NCEP/NCAR 40-Year Reanalysis Project. *Bull. Amer. Meteor. Soc.*, **77**, 437–471.

Keith, W. H., and J. M. O’Neal, 1967: A cloud climatology for selected Antarctic locations from November 1966, December 1966, and January 1967 meteorological satellite data. Navy Weather Research Facility, Norfolk, VA, 132 pp. [NTIS AD778300]

Keller, Linda M.; Weidner, George A.; Stearns, Charles R.; Thom, Jonathan E. and Lazzara, Matthew A., 2007: Antarctic Automatic Weather Station data for the calendar year 2001. University of Wisconsin-Madison, Space Science and Engineering Center, Madison, WI. Call Number: UW SSEC Publication No.07.02.K1

Kermann, W. O., and D. D. Frame, 1966: Antarctic temperature studies utilizing HRIR data from Nimbus I. M.S. thesis. Dept. of Meteorology, Naval Postgraduate School, 53 pp. [NTIS AD803350.]

Key, J. R., X. Wang, J.C. Stoeve, and C. Fowler, 2001: Estimating the cloudy-sky albedo of sea ice and snow from space. *J. Geophys. Res.*, **106**, 12,489-12,497.

King, J.C. and J. Turner, 1997: *Antarctic Meteorology and Climatology.* Cambridge University Press, 409 pp.

Lazzara, M.A., J.M. Benson, R.J. Fox, D.J. Laitsch, J.P. Rueden, D.A. Santek, D.M. Wade, T.M. Whittaker, and J.T. Young, 1999: The Man computer Interactive Data Access System: 25 Years of Interactive Processing. *Bull. Amer. Meteor. Soc.*, **80**, 271–284.

Lazzara, M. A., L. M. Keller, C. R. Stearns, J. E. Thom, G. A. Weidner, 2003a: Antarctic Satellite Meteorology: Applications for Weather Forecasting. *Mon. Wea. Rev.,* **131**, 371–383.

Lazzara, M.A., C.R. Stearns, J.A. Staude, and S.L. Knuth, 2003b: 10 Years of Antarctic Composite Imagery. 7th Polar Conference on Polar Meteorology and Oceanography and Joint Symposium on High-Latitude Climate Variations. AMS, 9.4.

Lazzara, M.A., 2005: Polar Environmental Monitoring, Communications, and Space Weather from Polar Sitter Orbit. UW SSEC Publication No.05.04.L1. Space Science and Engineering Center, University of Wisconsin-Madison, 10 pp. [Available from The Schwerdtfeger Library, University of Wisconsin-Madison, 1225 W. Dayton St., Madison,WI 53706.]

Limpasuvan, V., and D. L. Hartmann, 1999: Eddies and the annular modes of climate variability. *Geophys. Res. Lett.,* **26**, 3133-3166.

McBride, J. L., and N. Nicholls, 1983: Seasonal relationships between Australian rainfall and the Southern Oscillation. *Mon. Wea. Rev.* **111**, 517-528.

Menzel, W. P. and J. F. W. Purdom, 1994: Introducing GOES-I: The first of a new generation of Geostationary Operational Environmental Satellites. *Bull. Amer. Meteor. Soc.*, **75**, 757-781.

Rasmusson, Eugene M. and John M. Wallace, 1983: Meteorological Aspects of the El Niño/Southern Oscillation. *Science*, **222**, 1195-1202.

Rogers, J. C., and H. van Loon, 1982: Spatial Variability of sea level pressure and 500-mb height anomalies over the Southern Hemisphere. *Mon. Wea. Rev.*, **110**, 1375-1392.

Ropelewski, C. F., and P. D. Jones, 1987: An Extension of the Tahiti-Darwin Southern Oscillation Index. *Mon. Wea. Rev.,* **115**, 2161-2165.

Schwerdtfeger, W., 1984: Weather and Climate of the Antarctic. *Develop. Atm. Sci.,* **15**, Elsevier Science Publishers B. V., 262 pp.

Sinclair, M.R., J.A. Renwick, and J.W. Kidson, 1997: Low-Frequency Variability of Southern Hemisphere Sea Level Pressure and Weather System Activity. *Mon. Wea. Rev.*, **125**, 2531–2543.

Stearns, C.R., L. Keller, G.A. Weidner, and M. Sievers, 1993: Monthly mean climatic data for Antarctic automatic weather stations. Antarctic Research Series, *Amer. Geophys. Union*, **61**, 1-22.

Smith, S. R. and C. R. Stearns, 1993: Antarctic Climate Anomalies Surrounding the Minimum in the Southern Oscillation Index. Antarctic Research Series, *Amer. Geophys. Union*, **61**, 149-174.

Stearns, C.R., and Lazzara, M.A., 1999: Six Years of Composite Infra-red Images South of Forty South at Three Hourly Intervals. IUGG99 Conference, Birmingham, UK.

Taljaard, J. J., 1967: Development, distribution and movement of cyclones and anticyclones in the Southern Hemisphere during the IGY. *J. Appl. Meteor.,* **6**, 973-987.

Thompson, D. W. J., and J. M. Wallace, 2000: Annular modes in the extratropical circulation. Part I: Month-to-month variability. *J. Climate*, **13**, 1000-1016.

Trenberth, K. E., 1984: Signal versus noise in the Southern Oscillation. *Mon. Wea. Rev.*, **112**, 326-332.

——, 1997: The definition of El Niño. *Bull. Amer. Meteor. Soc*., **78**, 2771-2777.

Troup, A. J., 1965: The Southern Oscillation. *Quart. J. Roy. Meteor. Soc.*, **91**, 490-506.

Van Loon, H., 1979: The Association Between Latitudinal Temperature Gradient and Eddy Transport. Part I: Transport of Sensible Heat in Winter, *Mon. Wea. Rev.*, **107**, 525-534.

Walker, G. T., 1923: World Weather I. *Mem. India Met. Dept.*, **24**, 75.

——, 1924: World Weather II. *Ibid.*, **24**, 275.

——, 1928: World Weather. *Quart J. Roy. Meteor. Soc..*, **54**, 79-87.

Walker, G.T. and Bliss, E.W., 1928: World Weather III. Mem. *Royal Meteor*. Soc., **2**, 97.

——, 1932: World Weather V. Mem. *Royal Meteor*. Soc., **4**, 53-84.

——, 1937: World Weather VI, Mem., *Royal Meteor*. Soc., **4**, 119-139.

Wang, X. and J. R. Key, 2002: Arctic climate characteristics and recent trends based on the AVHRR Polar Pathfinder data set. IGARSS '02: 2002 International Geoscience and Remote Sensing Symposium proceedings, v.3. Piscataway, NJ: Institute of Electrical and Electronic Engineers, Inc., 1842-1844.

Wyckoff, Robert L., 2005. Hydrologic Dynamics of Climate and Land-use Change: Multiple - Resolution Modeling of the Rio Puerco River Basin, New Mexico. For the Water Resources Research Institute at the New Mexico State University, Las Cruces, NM. 25 pp.

8. Appendix of Figures

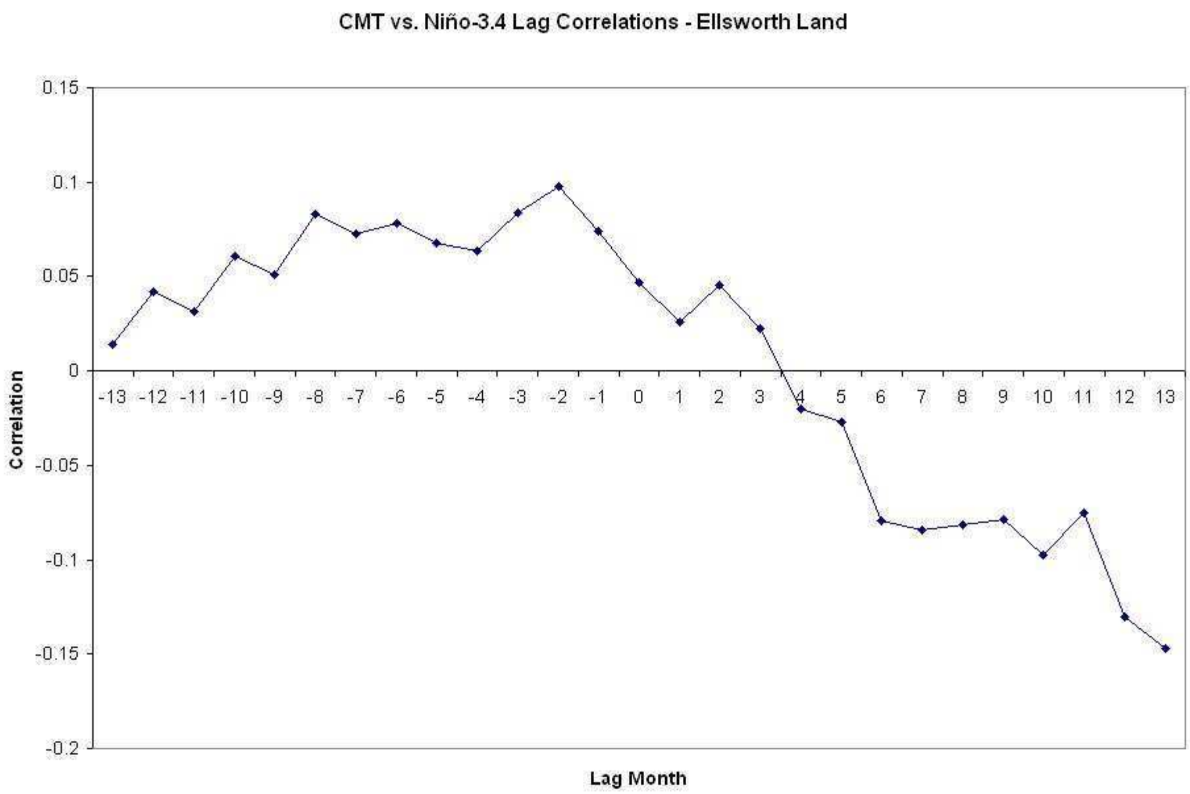

Figure 1. A plot of CMT vs. Niño-3.4 Lag Correlations for Ellsworth Land from months -13 to +13.

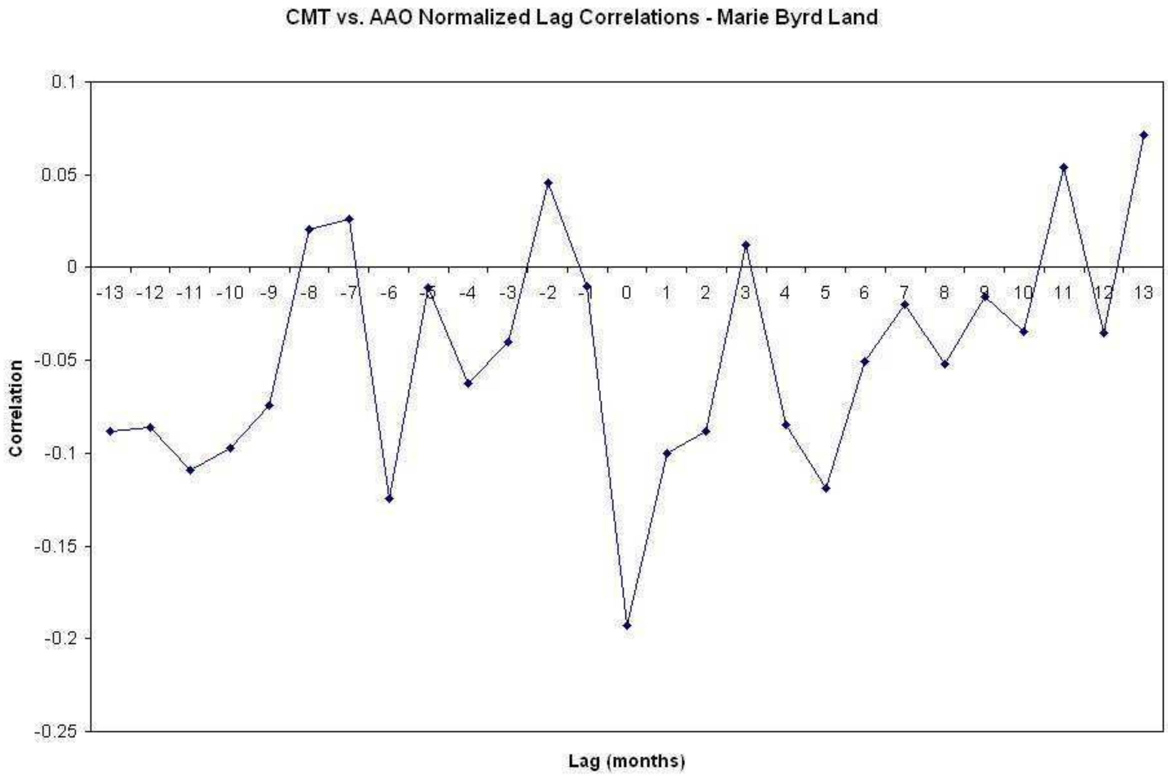

Figure 2. A plot of CMT vs. AAO Lag Correlations for Marie Byrd Land from months -13 to +13.

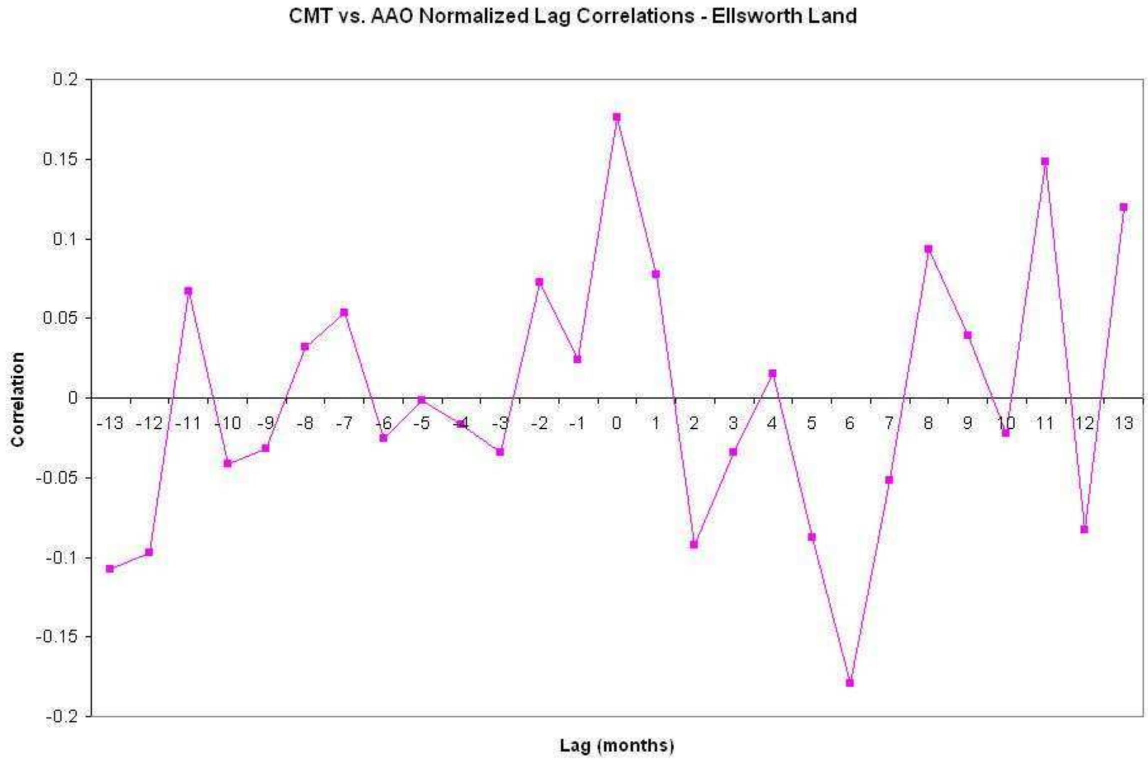

Figure 3. A plot of CMT vs. AAO Lag Correlations for Ellsworth Land from months -13 to +13.

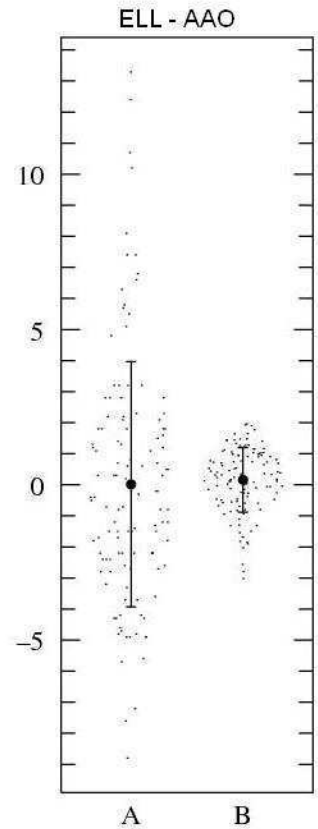

Figure 4. A whisker plot for Ellsworth Land and the AAO. The A whisker plot represents CMT events and B represents the AAO.

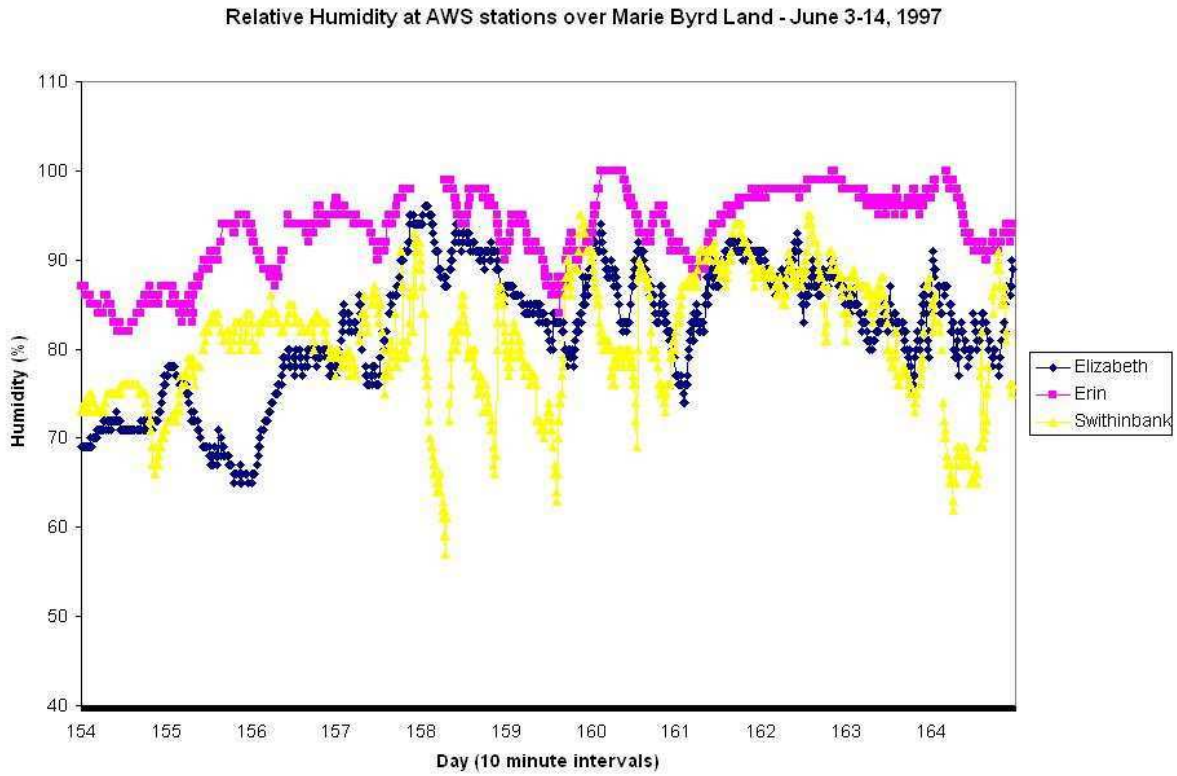

Figure 5. A plot showing relative humidity at three different AWS stations in Marie Byrd Land from June 3-14, 1997.

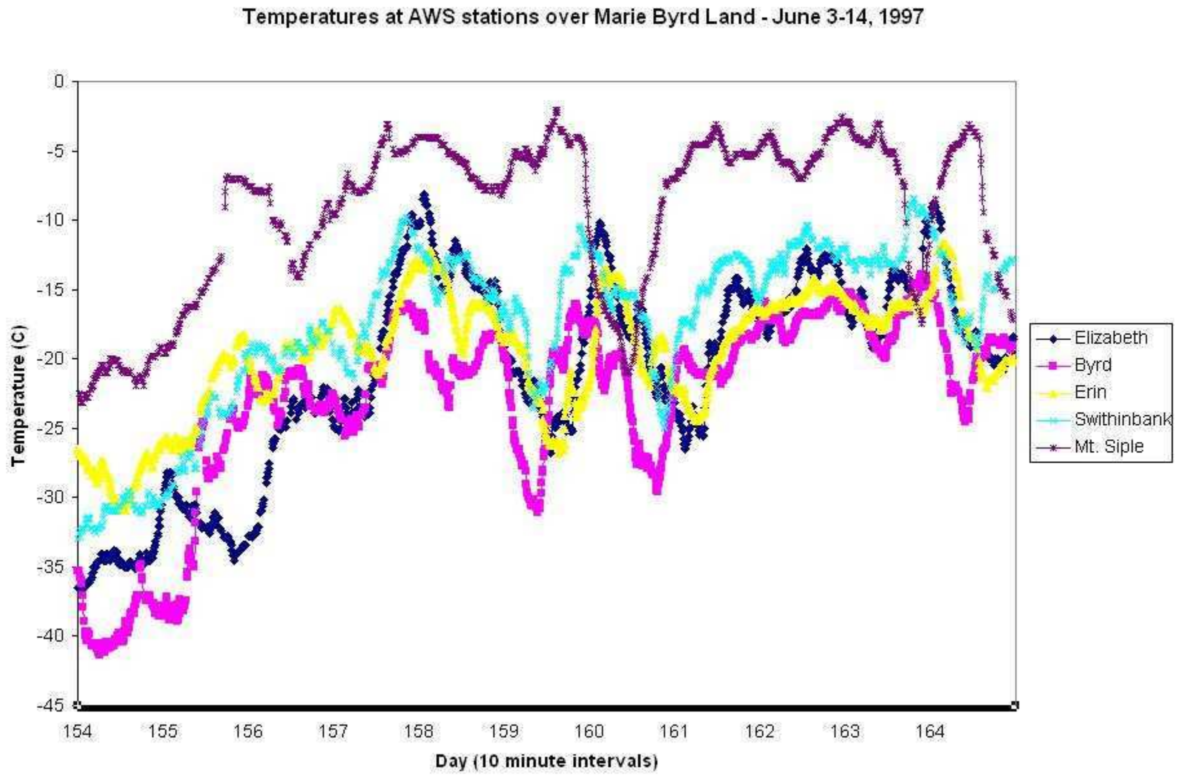

Figure 6. A plot showing temperatures at five different AWS stations in Marie Byrd Land from June 3-14, 1997.

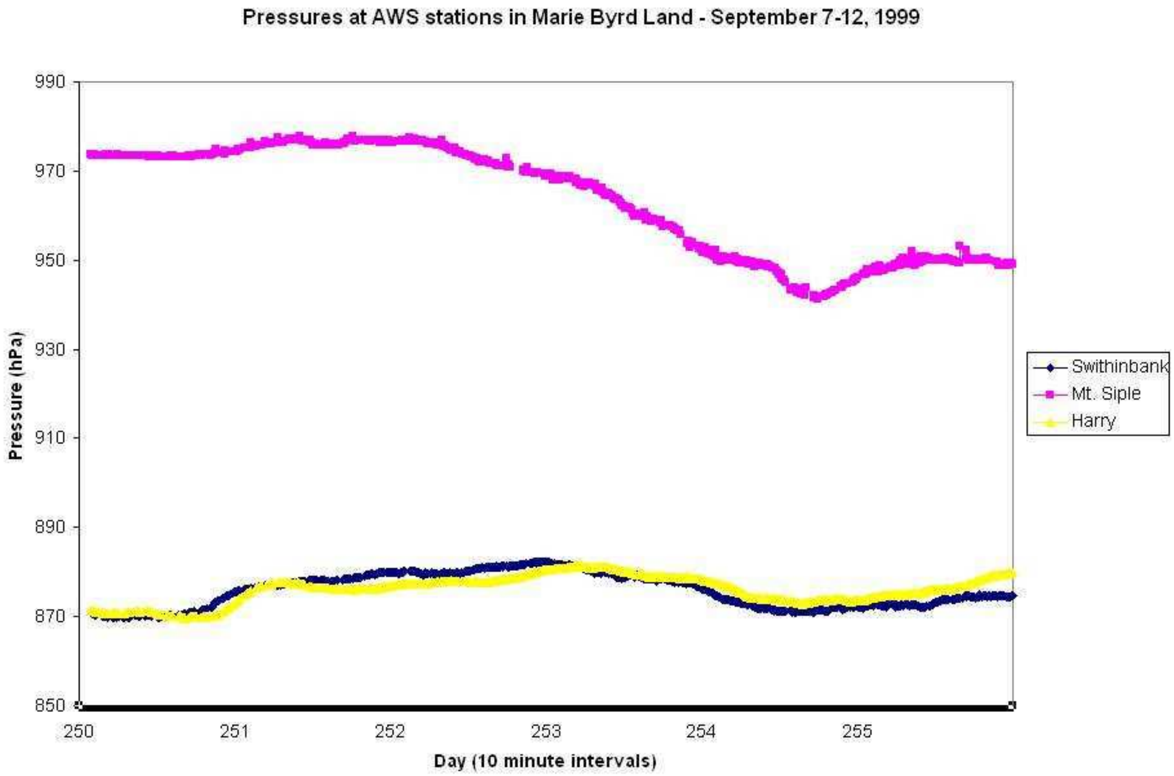

Figure 7. A plot showing pressures at three different AWS stations in Marie Byrd Land from September 7-12, 1999.

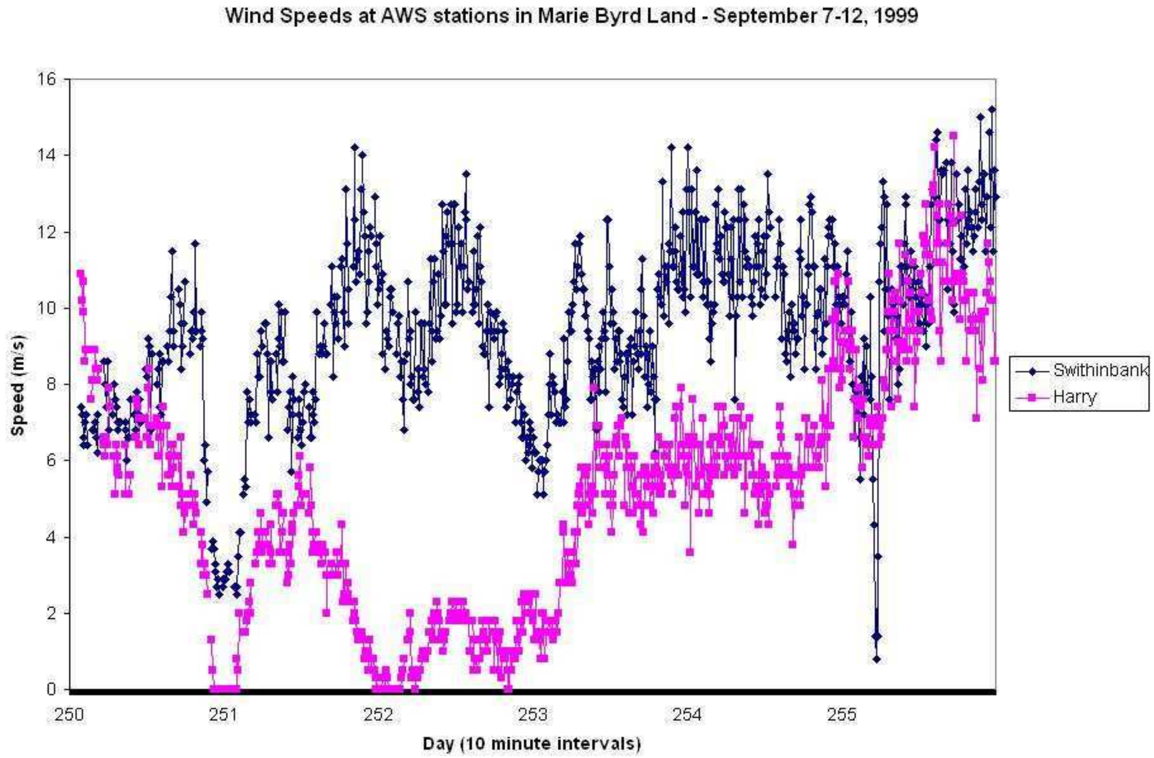

Figure 8. A plot showing wind speeds at two different AWS stations in Marie Byrd Land from September 7-12, 1999.

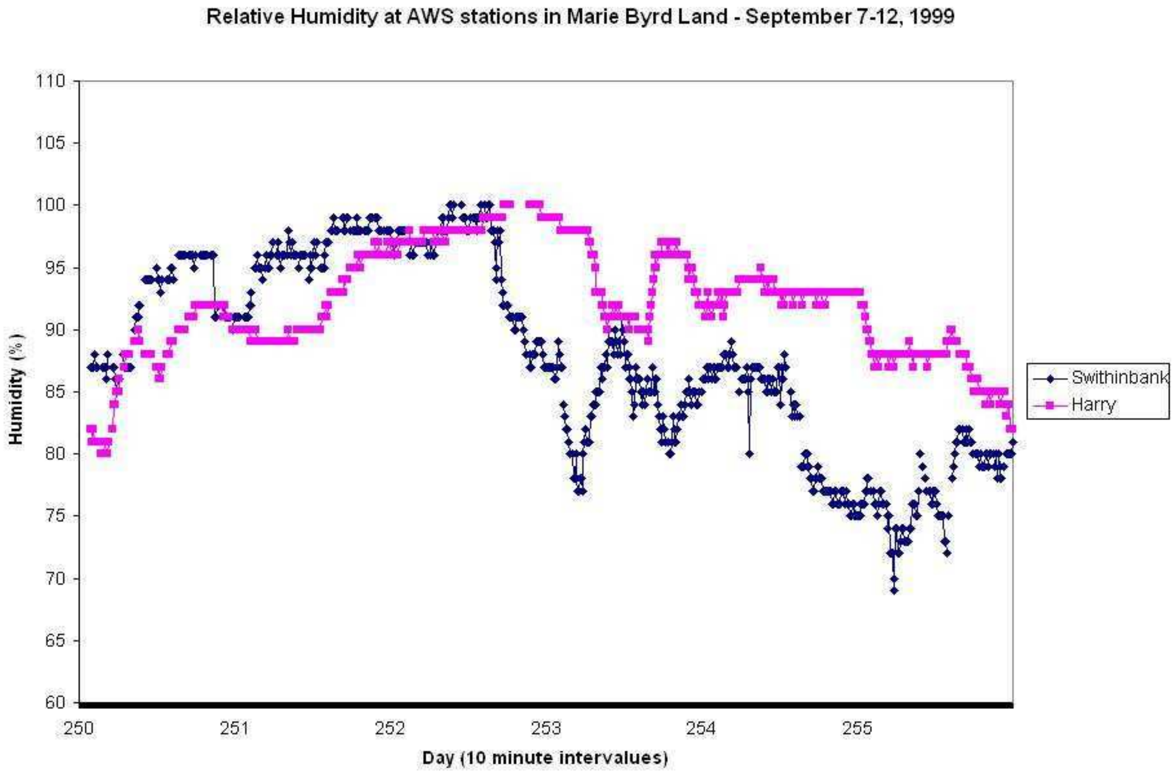

Figure 9. A plot showing relative humidity at two different AWS stations in Marie Byrd Land from September 7-12, 1999.

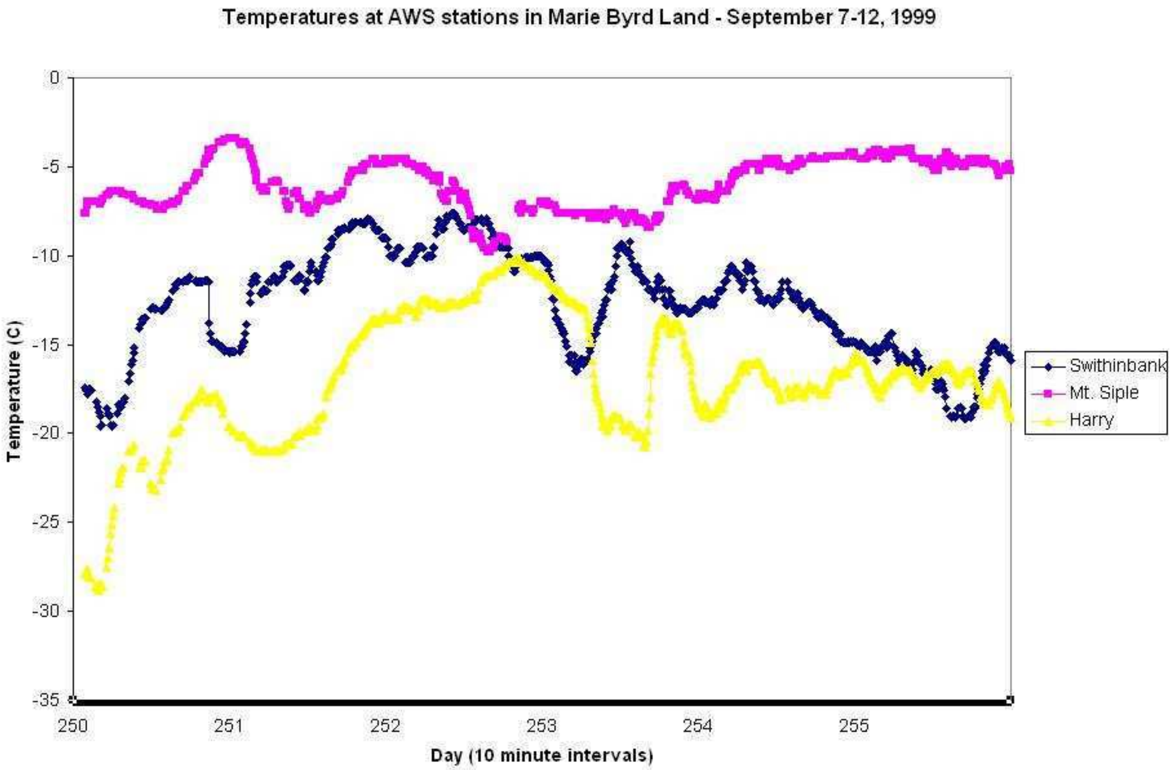

Figure 10. A plot showing temperatures at three different AWS stations in Marie Byrd Land from September 7-12, 1999.

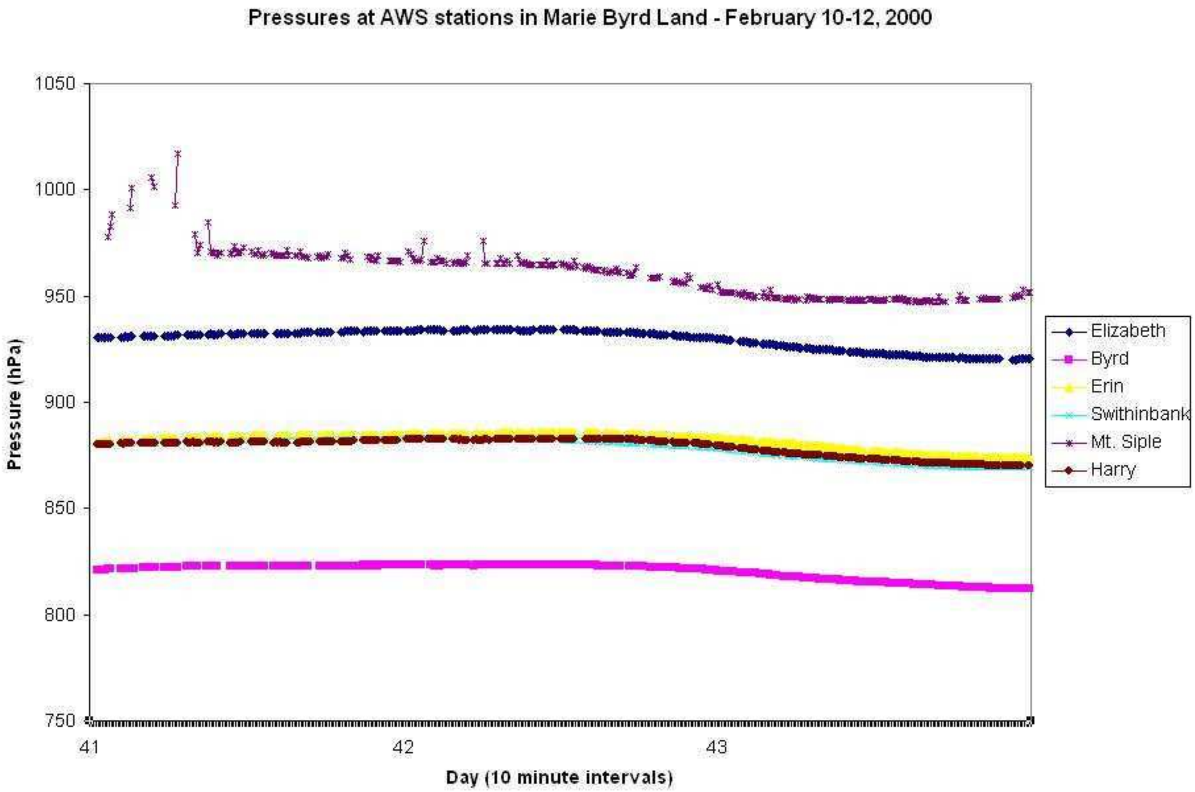

Figure 11. A plot showing pressures at six different AWS stations in Marie Byrd Land from February 10-12, 2000.

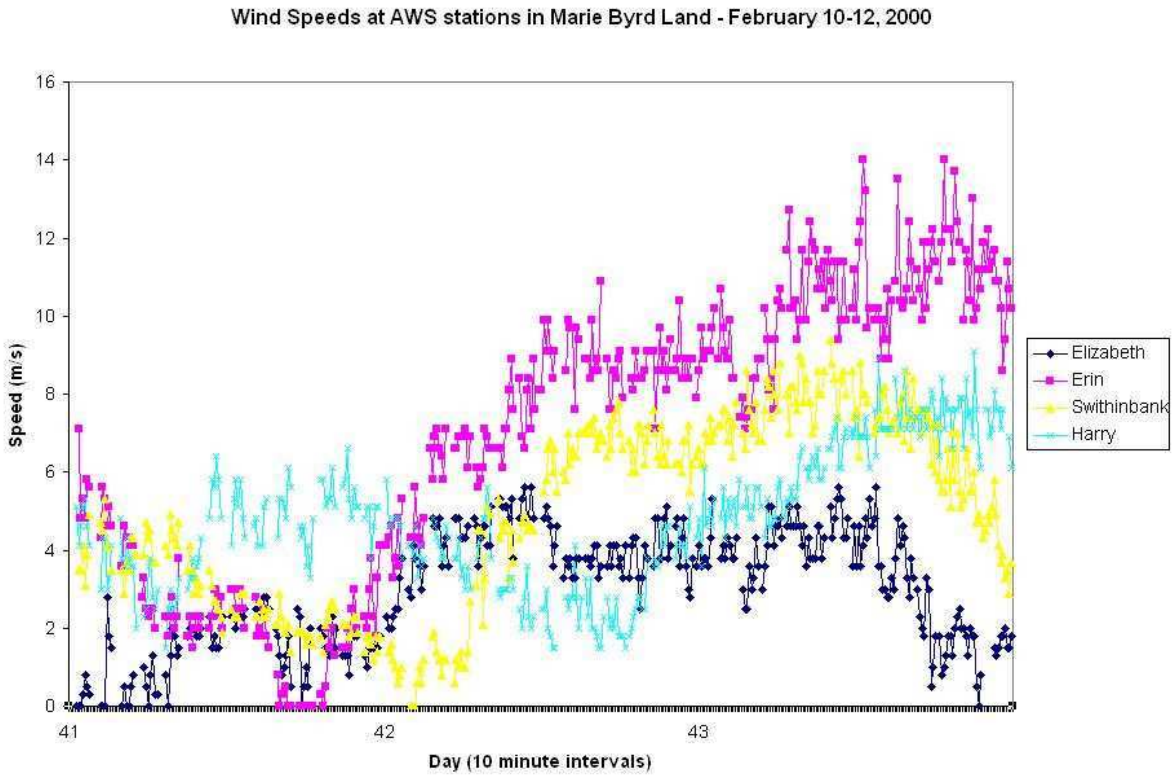

Figure 12. A plot showing wind speeds at four different AWS stations in Marie Byrd Land from February 10-12, 2000.

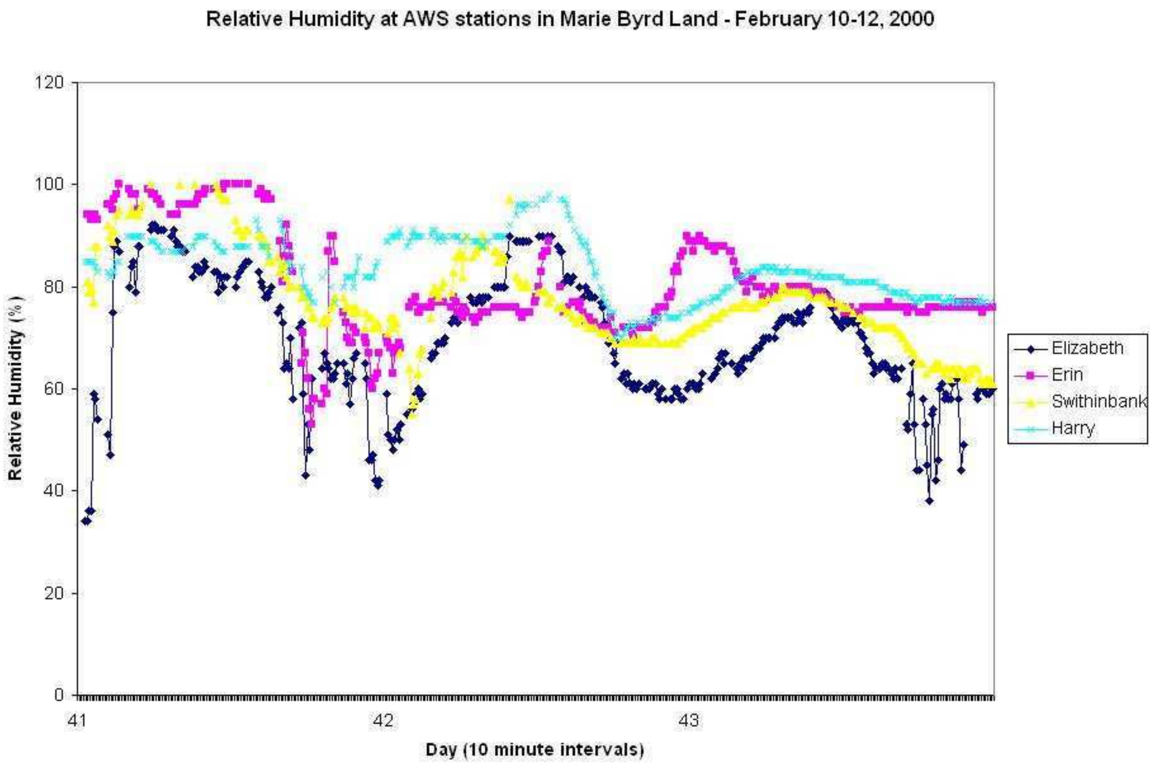

Figure 13. A plot showing relative humidity at four different AWS stations in Marie Byrd Land from February 10-12, 2000

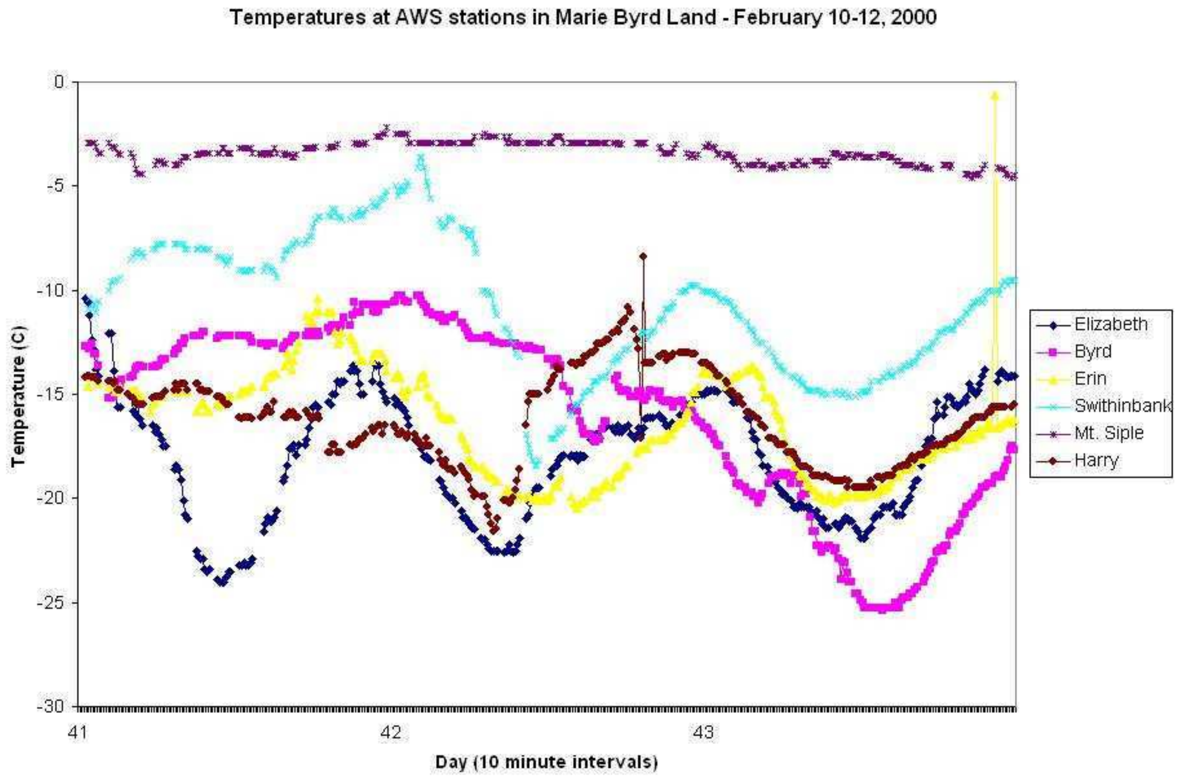

Figure 14. A plot showing temperatures at six different AWS stations in Marie Byrd Land from February 10-12, 2000.

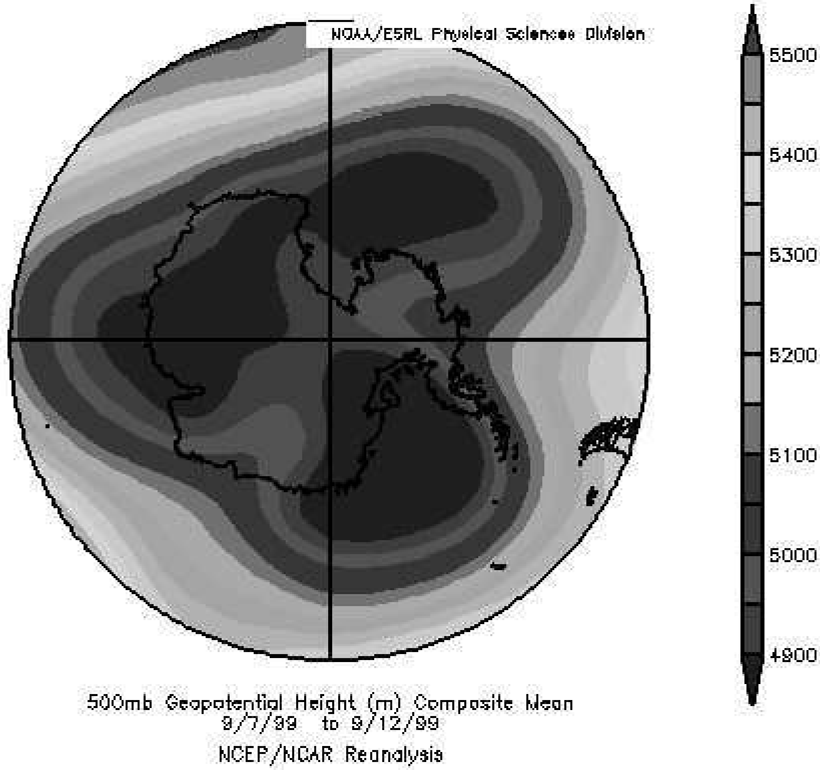

Figure 15. 500 hPa Geopotential heights calculated from daily NCEP/NCAR reanalysis data for the period September 7-12, 1999.

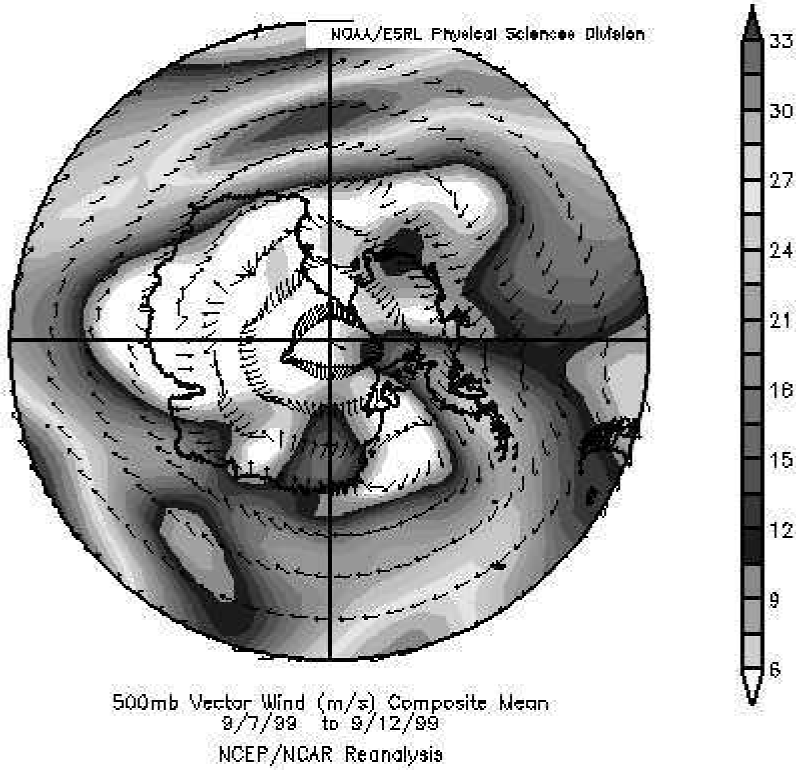

Figure 16. 500 hPa vector winds calculated from daily NCEP/NCAR reanalysis data for the period September 7-12, 1999.

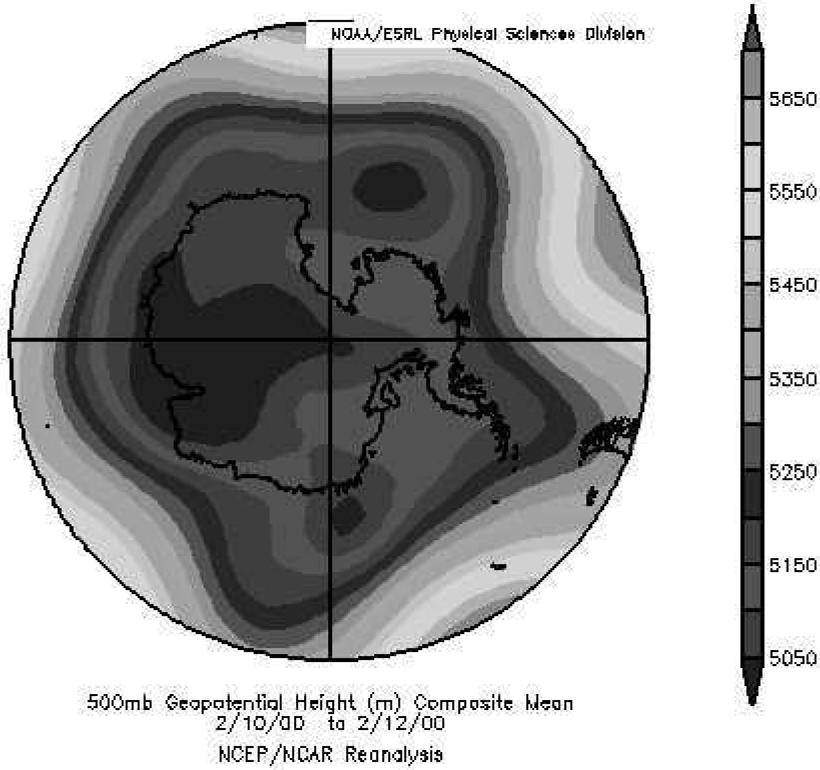

Figure 17. 500 hPa Geopotential heights calculated from daily NCEP/NCAR reanalysis data for the period February 10-12, 2000.

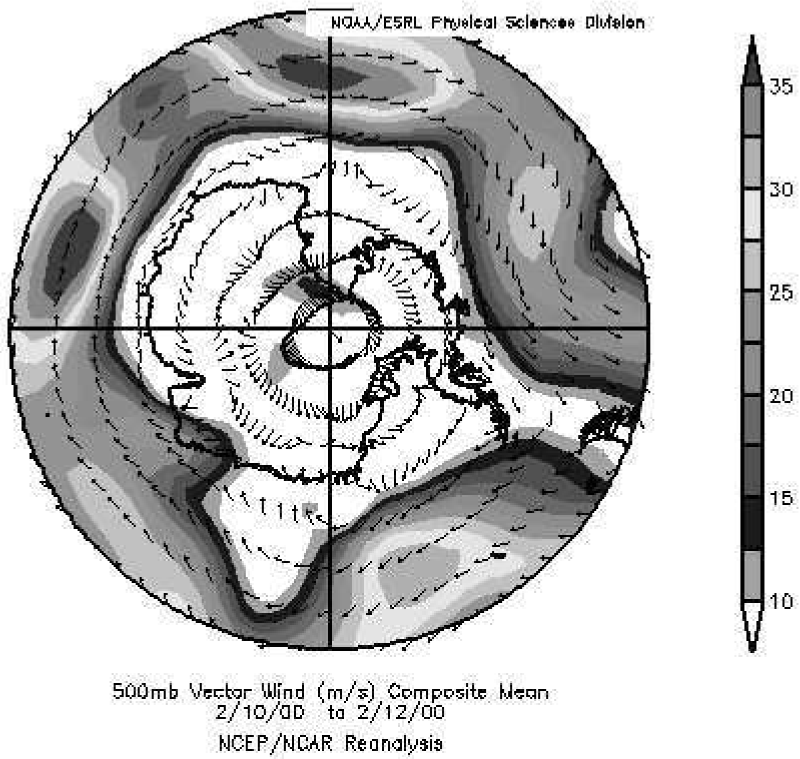

Figure 18. 500 hPa vector winds calculated from daily NCEP/NCAR reanalysis data for the period February 10-12, 2000.